

# Hybrid Beamforming for Intelligent Reflecting Surface Aided Millimeter Wave MIMO Systems

Sung Hyuck Hong, Jaeyong Park, Sung-Jin Kim, and Junil Choi

**Abstract**—While communication systems that employ millimeter wave (mmWave) frequency bands can support extremely high data rates, they must use large antenna arrays in order to overcome the severe propagation loss of mmWave signals. As the cost of traditional fully-digital beamforming at baseband increases rapidly with the number of antennas, hybrid beamforming that requires only a small number of radio frequency (RF) chains has been considered as a key enabling technology for mmWave communications. Intelligent reflecting surface (IRS) is another innovative technology that has been proposed as an integral element of future communication systems, establishing the favorable propagation environment in a timely manner through the use of low-cost passive reflecting elements. In this paper, we study IRS-aided mmWave multiple-input multiple-output (MIMO) systems with hybrid beamforming architectures. We first propose the joint design of IRS reflection pattern and hybrid beamformer for narrowband MIMO systems. Then, by exploiting the sparsity of frequency-selective mmWave channels in the angular domain, we generalize the proposed joint design to broadband MIMO systems with orthogonal frequency division multiplexing (OFDM) modulation. Simulation results demonstrate that the proposed joint designs can significantly enhance the spectral efficiency of the systems of interest and achieve superior performance over the existing designs.

**Index Terms**—Millimeter wave (mmWave) communications, multiple-input multiple-output (MIMO), hybrid beamforming, intelligent reflecting surface (IRS), frequency-selective channels, orthogonal frequency division multiplexing (OFDM).

## I. INTRODUCTION

**T**HE explosive growth in wireless data traffic and resultant issue of bandwidth shortage have increased the necessity of resorting to higher frequency bands that are relatively uncongested [1]. Since large bandwidth can be utilized at millimeter wave (mmWave) frequency bands to attain possibly up to gigabit-per-second data rates, mmWave communications have been viewed as one of the key technologies that can realize many new applications and services that the fifth generation (5G) wireless networks aim to support [2]. However, the propagation properties of mmWave signals, such as severe path loss and atmospheric attenuation, must be carefully examined in order to fully reap the expected benefits of mmWave communications [3], [4].

Massive multiple-input multiple-output (MIMO), the concept of utilizing a large number of antennas at the transceivers, has been proposed as a promising solution to combat the

high path loss of mmWave signals and achieve significant capacity gain through simultaneous transmission of multiple data streams [4], [5]. Despite its numerous advantages, massive MIMO makes the traditional fully-digital beamforming at baseband prohibitively expensive since such processing requires dedicated radio frequency (RF) chain for each antenna [6]. To address such issue, hybrid beamforming architectures that use the combination of a low-dimensional digital baseband beamformer and a high-dimensional analog beamformer have been proposed to increase the energy efficiency of massive MIMO systems, significantly reducing the number of RF chains at the cost of only slight performance degradation [7].

Many works have investigated mmWave MIMO communication systems with hybrid beamforming architectures [8]–[15]. In [8], the problem of designing hybrid precoders and combiners that maximize spectral efficiency was recast as a sparsity-constrained matrix reconstruction problem, which was subsequently solved using an algorithm based on orthogonal matching pursuit. Manifold optimization (MO)-based algorithms were proposed in [9] to tackle the hybrid precoder design problem in both narrowband and broadband mmWave MIMO systems. The authors in [10] presented a unified heuristic algorithm to design beamformers for frequency-selective mmWave channels under fully-connected and partially-connected hybrid architectures. Hybrid beamformer designs that aim to minimize mean square error (MSE) of data streams were proposed in [11]–[13], while some works considered the use of finite-resolution phase shifters in implementing analog beamformers [14], [15].

Recently, intelligent reflecting surface (IRS) has been proposed as a cost-effective and innovative technology to smartly reconfigure the wireless propagation environments in a real-time manner, thereby significantly improving the performance of future communication systems [16]. Labeled as one of the key components of sixth generation (6G) wireless networks, IRS is a metasurface consisting of a large number of passive reflecting elements, each of which induces an adjustable phase and/or amplitude shift to the incident electromagnetic waves [17], [18]. Since mmWave signals are highly vulnerable to blockages due to the narrow beamwidth, IRS is, along with massive MIMO and hybrid beamforming, expected to play a pivotal role in enhancing the coverage and spectral/energy efficiency of mmWave communication systems [18], [19].

As 6G wireless networks aim to provide even higher data rates and energy efficiency than 5G networks in which mmWave frequency bands are heavily employed, upcoming communication systems must integrate IRS into mmWave MIMO systems with large antenna arrays and hybrid beam-

Sung Hyuck Hong and Junil Choi are with the School of Electrical Engineering, Korea Advanced Institute of Science and Technology, Daejeon 34141, South Korea (e-mail: {shong16; junil}@kaist.ac.kr).

Jaeyong Park and Sung-Jin Kim are with C&M Standard Lab, Future Technology Center, LG Electronics Inc. (e-mail: {jaeyong630.park; sj88.kim}@lge.com).

forming architectures to successfully attain such performance targets [20], [21]. However, among the limited number of studies on the IRS reflection pattern design for point-to-point MIMO communications [22]–[27], only [26] and [27] considered mmWave MIMO systems with hybrid beamforming architectures. In [26], an iterative algorithm based on MO was developed to design the IRS reflection pattern and hybrid beamformer for frequency-flat mmWave channels. It is difficult, however, to extend the algorithm to frequency-selective channels, which are highly relevant to mmWave systems that tend to have large available bandwidth [9], [10]. Though applicable to broadband MIMO systems under frequency-selective channels, the hybrid beamformer design proposed in [27] focused on minimizing bit error rate (BER) and thus entails an inevitable loss in spectral efficiency. Furthermore, the hybrid beamformer designs in [26] and [27] did not take into account how the designed IRS reflection pattern influences the structure of mmWave channels, although doing so can lead to significant performance improvement and complexity reduction.

Motivated by these facts, we propose in this paper the joint designs of IRS reflection pattern and hybrid beamformer for narrowband and broadband mmWave MIMO systems. The proposed designs aim to maximize the spectral efficiency of IRS-aided mmWave MIMO systems, where a large number of antennas and passive reflecting elements are installed at the transceivers and IRS, respectively. To the best of our knowledge, this paper is the first to consider both the reflected channel from the transmitter (TX) to IRS to receiver (RX) and the direct channel from the TX to RX in IRS-aided mmWave MIMO systems with hybrid beamforming architectures. Our main contributions are summarized as follows:

- We develop an IRS reflection pattern design that successfully establishes the favorable communication environments for narrowband mmWave MIMO systems. Not resorting to any iterative procedure, the design will be highly useful in practical IRS-aided systems where IRS passive elements are deployed in large numbers.
- We propose a hybrid beamformer design that exploits the inherent structure of mmWave channels so as to attain the performance close to that of fully-digital beamforming. By carefully examining how the channels are adjusted according to the proposed IRS reflection pattern design, we construct hybrid precoders and combiners that fully reap considerable spectral efficiency gains offered by IRS.
- We generalize the proposed joint design of IRS reflection pattern and hybrid beamformer for narrowband MIMO systems to broadband MIMO systems with orthogonal frequency division multiplexing (OFDM) modulation. Smartly leveraging the sparsity of frequency-selective mmWave channels in the angular domain, the generalized design can significantly enhance the spectral and energy efficiency of IRS-aided MIMO-OFDM systems.

The rest of the paper is organized as follows. The system model and problem formulation are described in Section II. The joint design of IRS reflection pattern and hybrid beamformer for narrowband MIMO systems is proposed in Section

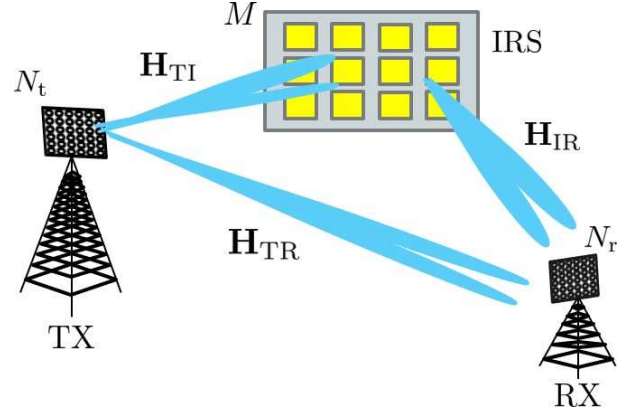


Fig. 1. Illustration of an IRS-aided mmWave MIMO system.

III. In Section IV, the proposed joint design is extended to broadband MIMO-OFDM systems. The complexity analysis and simulation results are presented in Section V and Section VI, respectively. Finally, conclusions are drawn in Section VII.

**Notation:** Vectors and matrices are represented by lower and upper boldface letters. The  $m \times n$  matrix whose elements are all zero is represented by  $\mathbf{0}^{m \times n}$ , while  $\mathbb{C}^{m \times n}$  denotes the set of all  $m \times n$  complex matrices. The transpose, conjugate transpose, inverse, determinant, and rank of the matrix  $\mathbf{A}$  are represented by  $\mathbf{A}^T$ ,  $\mathbf{A}^H$ ,  $\mathbf{A}^{-1}$ ,  $\det(\mathbf{A})$ , and  $\text{rank}(\mathbf{A})$ , respectively. The Frobenius norm of  $\mathbf{A}$  is denoted by  $\|\mathbf{A}\|_F$ , while  $\text{row}(\mathbf{A})$  and  $\text{col}(\mathbf{A})$  indicate the number of rows and columns of  $\mathbf{A}$ , respectively. The element in the  $i$ -th row and  $j$ -th column of  $\mathbf{A}$  is denoted by  $[\mathbf{A}]_{i,j}$ , whereas  $[\mathbf{A}]_{:,j}$  represents the  $j$ -th column vector of  $\mathbf{A}$ . Similarly,  $[\mathbf{A}]_{:,1:j} \in \mathbb{C}^{\text{row}(\mathbf{A}) \times j}$  and  $[\mathbf{A}]_{1:j,1:j} \in \mathbb{C}^{j \times j}$  each denote the matrix whose columns are given by the first  $j$  columns of  $\mathbf{A}$  and that consisting of the first  $j$  rows and columns of  $\mathbf{A}$ . The  $j$ -th element of the vector  $\mathbf{x}$  is denoted by  $[\mathbf{x}]_j$ , while  $\text{diag}(\mathbf{x})$  represents the diagonal matrix that contains the elements of  $\mathbf{x}$  on its main diagonal. The  $N \times N$  identity matrix and the expectation operator are represented by  $\mathbf{I}_N$  and  $\mathbb{E}[\cdot]$ , respectively. The function  $\max(a, 0)$  defined for a real number  $a$  is denoted by  $(a)^+$ , whereas  $|\cdot|$  and  $\|\cdot\|_2$  each indicate the absolute value of a scalar and the  $\ell_2$ -norm of a vector. The complex and real normal distributions with mean  $m$  and variance  $\sigma^2$  are denoted by  $\mathcal{CN}(m, \sigma^2)$  and  $\mathcal{N}(m, \sigma^2)$ , respectively.

## II. SYSTEM MODEL AND PROBLEM FORMULATION

In this paper, we consider an IRS-aided mmWave MIMO system with a hybrid beamforming architecture. For the sake of simplicity, we first describe a narrowband system in this section, and introduce a broadband system later in Section IV. As shown in Fig. 1, an IRS consisting of  $M$  passive reflecting elements assists the communication between the TX with  $N_t$  antennas and the RX with  $N_r$  antennas. Let  $\mathbf{H}_{\text{TR}} \in \mathbb{C}^{N_r \times N_t}$  denote the direct channel from the TX to RX. Similarly, let  $\mathbf{H}_{\text{TI}} \in \mathbb{C}^{M \times N_t}$  and  $\mathbf{H}_{\text{IR}} \in \mathbb{C}^{N_r \times M}$  represent the channel from the TX to IRS and that from the IRS to RX, respectively. With each reflecting element

of the IRS serving as a single point source that scatters the received signal after applying to it a controllable phase shift, the effect of IRS can be modeled by the diagonal matrix  $\Phi = \text{diag}([e^{j\theta_1}, \dots, e^{j\theta_M}]) \in \mathbb{C}^{M \times M}$ , where  $\theta_m \in [0, 2\pi)$  denotes the phase shift of  $m$ -th IRS element,  $m \in \{1, \dots, M\}$  [16], [17]. The total combined channel from the TX to RX can then be expressed as  $\mathbf{H}_{\text{tot}} = \mathbf{H}_{\text{TR}} + \mathbf{H}_{\text{IR}}\Phi\mathbf{H}_{\text{TI}}$ .

The TX sends  $N_s$  data streams to the RX using the digital baseband precoder  $\mathbf{F}_{\text{BB}} \in \mathbb{C}^{N_t^{\text{RF}} \times N_s}$  and analog precoder  $\mathbf{F}_{\text{RF}} \in \mathbb{C}^{N_t \times N_t^{\text{RF}}}$ , where the number of RF chains at the TX is denoted by  $N_t^{\text{RF}}$  and is subject to the constraint  $N_s \leq N_t^{\text{RF}} \leq N_t$ . We impose the total power constraint  $P_{\text{TX}}$  on the transmit power, i.e.,  $\|\mathbf{F}_{\text{RF}}\mathbf{F}_{\text{BB}}\|_{\text{F}}^2 \leq P_{\text{TX}}$ . The RX uses the analog combiner  $\mathbf{W}_{\text{RF}} \in \mathbb{C}^{N_r \times N_r^{\text{RF}}}$  and digital baseband combiner  $\mathbf{W}_{\text{BB}} \in \mathbb{C}^{N_r^{\text{RF}} \times N_s}$  to process the received signal, where the number of RF chains at the RX  $N_r^{\text{RF}}$  is subject to the constraint  $N_s \leq N_r^{\text{RF}} \leq N_r$ . As the analog combiner  $\mathbf{W}_{\text{RF}}$  and precoder  $\mathbf{F}_{\text{RF}}$  are implemented with phase shifters, the constant modulus constraint is imposed on each of their elements, i.e.,  $|\mathbf{W}_{\text{RF}}[m,n]| = 1/\sqrt{N_r}$ ,  $|\mathbf{F}_{\text{RF}}[m,n]| = 1/\sqrt{N_t}$ ,  $\forall m, n$ . The processed received signal is expressed as

$$\tilde{\mathbf{y}} = \mathbf{W}_{\text{BB}}^H \mathbf{W}_{\text{RF}}^H \mathbf{H}_{\text{tot}} \mathbf{F}_{\text{RF}} \mathbf{F}_{\text{BB}} \mathbf{s} + \mathbf{W}_{\text{BB}}^H \mathbf{W}_{\text{RF}}^H \mathbf{n}, \quad (1)$$

where  $\mathbf{s} \in \mathbb{C}^{N_s \times 1}$  is the symbol vector satisfying  $\mathbb{E}[\mathbf{s}\mathbf{s}^H] = \mathbf{I}_{N_s}$ , and  $\mathbf{n} \in \mathbb{C}^{N_r \times 1}$  is an additive white Gaussian noise (AWGN) vector whose entries are independently and identically distributed (i.i.d) with  $\mathcal{CN}(0, \sigma_n^2)$ . To accurately evaluate the effectiveness of the proposed IRS reflection pattern and hybrid beamformer design, we assume in this paper that perfect channel state information (CSI) is available at the TX and RX [8]–[10], [19], [24]–[27]. The achievable spectral efficiency when the transmitted symbols follow a Gaussian distribution is given by

$$R = \log_2 \det(\mathbf{I}_{N_s} + \mathbf{R}_{\bar{\mathbf{n}}}^{-1} \mathbf{W}_{\text{BB}}^H \mathbf{W}_{\text{RF}}^H \mathbf{H}_{\text{tot}} \mathbf{F}_{\text{RF}} \mathbf{F}_{\text{BB}} \times \mathbf{F}_{\text{BB}}^H \mathbf{F}_{\text{RF}}^H \mathbf{H}_{\text{tot}}^H \mathbf{W}_{\text{RF}} \mathbf{W}_{\text{BB}}), \quad (2)$$

where  $\mathbf{R}_{\bar{\mathbf{n}}} = \sigma_n^2 \mathbf{W}_{\text{BB}}^H \mathbf{W}_{\text{RF}}^H \mathbf{W}_{\text{RF}} \mathbf{W}_{\text{BB}}$  represents the covariance matrix of the noise  $\bar{\mathbf{n}} = \mathbf{W}_{\text{BB}}^H \mathbf{W}_{\text{RF}}^H \mathbf{n}$  after combining.

Throughout this paper, we adopt the widely used Saleh-Valenzuela model [8], [9], [11]–[14], [26], [27] to represent mmWave channels. Each of the narrowband mmWave channels is expressed as

$$\mathbf{H}_i = \sum_{q=0}^{N_{\text{path}}^i - 1} \alpha_{i,q} \mathbf{a}_r(\phi_{i,q}^r, \theta_{i,q}^r) \mathbf{a}_t(\phi_{i,q}^t, \theta_{i,q}^t)^H, \quad (3)$$

where  $i \in \{\text{TR}, \text{TI}, \text{IR}\}$  is the subscript for the channel matrices,  $N_{\text{path}}^i$  is the number of physical propagation paths in  $\mathbf{H}_i$ , and  $\alpha_{i,q}$  is the complex gain of the  $q$ -th path in  $\mathbf{H}_i$ . We assume that  $\alpha_{i,q}$  are independently distributed with  $\mathcal{CN}(0, \gamma_i^2 10^{-0.1 PL(d_i)})$ ,  $\forall q \in \{0, \dots, N_{\text{path}}^i - 1\}$ , where  $\gamma_i = \sqrt{\text{row}(\mathbf{H}_i)\text{col}(\mathbf{H}_i)/N_{\text{path}}^i}$  is the normalization factor, and  $PL(d_i)$  represents the path loss that depends on the distance  $d_i$  between the two entities associated with  $\mathbf{H}_i$  [28]. For example,  $d_{\text{TR}}$  denotes the distance between the TX and RX. Lastly, the normalized receive and transmit array response vectors corresponding to the  $q$ -th path in  $\mathbf{H}_i$  are respectively denoted

by  $\mathbf{a}_r(\phi_{i,q}^r, \theta_{i,q}^r) \in \mathbb{C}^{\text{row}(\mathbf{H}_i) \times 1}$  and  $\mathbf{a}_t(\phi_{i,q}^t, \theta_{i,q}^t) \in \mathbb{C}^{\text{col}(\mathbf{H}_i) \times 1}$ , where  $\phi_{i,q}^r(\theta_{i,q}^r)$  and  $\phi_{i,q}^t(\theta_{i,q}^t)$  each stand for the azimuth (elevation) angles of arrivals and departures (AoAs and AoDs) of the path.

We assume in this paper that uniform planar arrays (UPAs) are employed at the TX, RX, and IRS. For the sake of clarity, set  $i = \text{TR}$  and define  $s \in \{0, \dots, N_{\text{path}}^{\text{TR}} - 1\}$ . The transmit array response vector  $\mathbf{a}_t(\phi_{\text{TR},s}^t, \theta_{\text{TR},s}^t) \in \mathbb{C}^{N_t \times 1}$  corresponding to the  $s$ -th path in  $\mathbf{H}_{\text{TR}}$  is then given by

$$\begin{aligned} & \mathbf{a}_t(\phi_{\text{TR},s}^t, \theta_{\text{TR},s}^t) \\ &= \frac{1}{\sqrt{N_t}} \left[ 1, \dots, e^{j \frac{2\pi d}{\lambda} (i_h \sin(\phi_{\text{TR},s}^t) \sin(\theta_{\text{TR},s}^t) + i_v \cos(\theta_{\text{TR},s}^t))}, \right. \\ & \quad \left. \dots, e^{j \frac{2\pi d}{\lambda} ((N_t^h - 1) \sin(\phi_{\text{TR},s}^t) \sin(\theta_{\text{TR},s}^t) + (N_t^v - 1) \cos(\theta_{\text{TR},s}^t))} \right]^T, \end{aligned} \quad (4)$$

where  $\lambda$  is the signal wavelength, and  $d$  is the spacing between the antennas or IRS elements. The horizontal and vertical indices for the transmit antennas are respectively denoted by  $0 \leq i_h < N_t^h$  and  $0 \leq i_v < N_t^v$ , where  $N_t = N_t^h N_t^v$ . Other receive and transmit array response vectors can be similarly defined.

In this paper, we aim to maximize the spectral efficiency in (2) by jointly designing the IRS reflection matrix  $\Phi$ , hybrid precoder  $\mathbf{F}_{\text{RF}}\mathbf{F}_{\text{BB}}$ , and hybrid combiner  $\mathbf{W}_{\text{RF}}\mathbf{W}_{\text{BB}}$ . The problem of maximizing the spectral efficiency is formulated as

$$(P1) \quad \max_{\mathbf{W}_{\text{BB}}, \mathbf{W}_{\text{RF}}, \Phi, \mathbf{F}_{\text{BB}}, \mathbf{F}_{\text{RF}}} R \quad (5a)$$

$$\text{subject to} \quad \Phi = \text{diag}([e^{j\theta_1}, \dots, e^{j\theta_M}]), \quad (5b)$$

$$\|\mathbf{F}_{\text{RF}}\mathbf{F}_{\text{BB}}\|_{\text{F}}^2 \leq P_{\text{TX}}, \quad (5c)$$

$$|\mathbf{W}_{\text{RF}}[m,n]| = 1/\sqrt{N_r}, \quad \forall m, n, \quad (5d)$$

$$|\mathbf{F}_{\text{RF}}[m,n]| = 1/\sqrt{N_t}, \quad \forall m, n. \quad (5e)$$

It is challenging to obtain the solution of the optimization problem (P1) since the constant modulus constraints (5b), (5d), (5e) on  $\Phi$ ,  $\mathbf{W}_{\text{RF}}$ , and  $\mathbf{F}_{\text{RF}}$  are non-convex. Additionally, the objective function  $R$ , which is coupled with the five matrix variables  $\{\mathbf{W}_{\text{BB}}, \mathbf{W}_{\text{RF}}, \Phi, \mathbf{F}_{\text{BB}}, \mathbf{F}_{\text{RF}}\}$ , is neither convex nor concave and thus makes the problem (P1) intractable to solve. To tackle these challenges, we reformulate the problem (P1) by exploiting its structure in the next section.

### III. JOINT DESIGN OF IRS REFLECTION PATTERN AND HYBRID BEAMFORMER

In this section, we propose the joint design of IRS reflection pattern and hybrid beamformer for narrowband mmWave MIMO systems described in Section II. Effectively exploiting the angular sparsity and large dimension of mmWave MIMO channels, the proposed design provides the systems of interest with significant increases in spectral efficiency.

#### A. Formulation of Effective Channel Design Problem

In this subsection, we transform (P1) into the effective channel design problem, whose purpose is to properly construct the analog combiner  $\mathbf{W}_{\text{RF}}$ , IRS reflection matrix  $\Phi$ ,

and analog precoder  $\mathbf{F}_{\text{RF}}$  so that the effective channel  $\mathbf{H}_{\text{eff}} = \mathbf{W}_{\text{RF}}^{\text{H}} \mathbf{H}_{\text{tot}} \mathbf{F}_{\text{RF}}$  is capable of supporting high spectral efficiency. We first re-express the objective function  $R$  of (P1) as

$$R = \log_2 \det(\mathbf{I}_{N_s} + \mathbf{R}_{\text{n}}^{-1} \mathbf{W}_{\text{BB}}^{\text{H}} \mathbf{H}_{\text{eff}} \mathbf{F}_{\text{BB}} \mathbf{F}_{\text{BB}}^{\text{H}} \mathbf{H}_{\text{eff}}^{\text{H}} \mathbf{W}_{\text{BB}}), \quad (6)$$

where  $\mathbf{H}_{\text{eff}} = \mathbf{W}_{\text{RF}}^{\text{H}} \mathbf{H}_{\text{tot}} \mathbf{F}_{\text{RF}}$  represents the effective channel after analog precoding and combining are applied. The expression in (6) shows that, when  $\mathbf{H}_{\text{eff}}$  is given, i.e., when  $\Phi$ ,  $\mathbf{W}_{\text{RF}}$ , and  $\mathbf{F}_{\text{RF}}$  are chosen to satisfy the constraints in (5b), (5d), and (5e), the problem (P1) can be simplified as

$$(P2) \quad \max_{\mathbf{W}_{\text{BB}}, \mathbf{F}_{\text{BB}}} \log_2 \det(\mathbf{I}_{N_s} + \mathbf{R}_{\text{n}}^{-1} \mathbf{W}_{\text{BB}}^{\text{H}} \mathbf{H}_{\text{eff}} \mathbf{F}_{\text{BB}} \mathbf{F}_{\text{BB}}^{\text{H}} \mathbf{H}_{\text{eff}}^{\text{H}} \mathbf{W}_{\text{BB}}) \quad (7a)$$

$$\text{subject to} \quad \|\mathbf{F}_{\text{RF}} \mathbf{F}_{\text{BB}}\|_{\text{F}}^2 \leq P_{\text{TX}}. \quad (7b)$$

Although not known in general, the optimal solution of the problem (P2) is given by  $\{\mathbf{W}_{\text{BB}} = \hat{\mathbf{W}}_{\text{BB}}, \mathbf{F}_{\text{BB}} = \hat{\mathbf{F}}_{\text{BB}}\}$  under the condition that  $\mathbf{W}_{\text{RF}}^{\text{H}} \mathbf{W}_{\text{RF}} = \mathbf{I}_{N_{\text{r}}^{\text{RF}}}$  and  $\mathbf{F}_{\text{RF}}^{\text{H}} \mathbf{F}_{\text{RF}} = \mathbf{I}_{N_{\text{t}}^{\text{RF}}}$  hold, where

$$\hat{\mathbf{W}}_{\text{BB}} = [\mathbf{U}_{\text{eff}}]_{:,1:N_s}, \quad \hat{\mathbf{F}}_{\text{BB}} = [\mathbf{V}_{\text{eff}}]_{:,1:N_s} \mathbf{P}_{\text{eff}}^{1/2}. \quad (8)$$

In (8),  $\mathbf{U}_{\text{eff}} \in \mathbb{C}^{N_{\text{r}}^{\text{RF}} \times N_{\text{r}}^{\text{RF}}}$  and  $\mathbf{V}_{\text{eff}} \in \mathbb{C}^{N_{\text{t}}^{\text{RF}} \times N_{\text{t}}^{\text{RF}}}$  each denote the unitary matrices whose columns are the left and right singular vectors of  $\mathbf{H}_{\text{eff}}$ , i.e., the singular value decomposition (SVD) of  $\mathbf{H}_{\text{eff}}$  is expressed as  $\mathbf{H}_{\text{eff}} = \mathbf{U}_{\text{eff}} \Sigma_{\text{eff}} \mathbf{V}_{\text{eff}}^{\text{H}}$ , where  $|\Sigma_{\text{eff}}]_{m,m}| \geq |\Sigma_{\text{eff}}]_{n,n}|, \forall m, n \in \{1, \dots, \min(N_{\text{r}}^{\text{RF}}, N_{\text{t}}^{\text{RF}})\}$  such that  $m < n$ . From now on, unless otherwise stated, we will express the SVD of a matrix such that its singular values are in descending order of their absolute values, just as in  $\Sigma_{\text{eff}}$ . The waterfilling power allocation matrix  $\mathbf{P}_{\text{eff}}^{1/2}$  for  $\mathbf{H}_{\text{eff}}$  is given by  $\mathbf{P}_{\text{eff}}^{1/2} = \text{diag}([\sqrt{P_1}, \dots, \sqrt{P_{N_s}}])$ , where  $P_l = \left(\frac{1}{\eta} - \frac{\sigma_n^2}{|\Sigma_{\text{eff}}]_{l,l}|^2}\right)^+$ ,  $\forall l \in \{1, \dots, N_s\}$ , and  $\eta$  is chosen such that  $\sum_{l=1}^{N_s} P_l = P_{\text{TX}}$ . The result in (8) indicates that, when the additional constraint is imposed on (P1) so that each of  $\mathbf{W}_{\text{RF}}$  and  $\mathbf{F}_{\text{RF}}$  has orthonormal columns, the baseband combiner  $\hat{\mathbf{W}}_{\text{BB}}$  and precoder  $\hat{\mathbf{F}}_{\text{BB}}$  maximize the spectral efficiency  $R$  in (2) for given  $\mathbf{W}_{\text{RF}}$ ,  $\Phi$ , and  $\mathbf{F}_{\text{RF}}$ . In fact,  $\hat{\mathbf{W}}_{\text{BB}}$  and  $\hat{\mathbf{F}}_{\text{BB}}$  achieve the maximum spectral efficiency<sup>1</sup>  $R_{\text{max}}(\mathbf{H}_{\text{eff}})$  that can be attained under  $\mathbf{H}_{\text{eff}}$ , i.e.,

$$R \Big|_{\substack{\mathbf{W}_{\text{BB}} = \hat{\mathbf{W}}_{\text{BB}} \\ \mathbf{F}_{\text{BB}} = \hat{\mathbf{F}}_{\text{BB}}} = \sum_{l=1}^{N_s} \log_2 \left( 1 + \frac{P_l}{\sigma_n^2} |\Sigma_{\text{eff}}]_{l,l}|^2 \right) = R_{\text{max}}(\mathbf{H}_{\text{eff}}). \quad (9)$$

We therefore aim to maximize  $R_{\text{max}}(\mathbf{H}_{\text{eff}})$  in (9) by properly designing  $\mathbf{W}_{\text{RF}}$ ,  $\Phi$ , and  $\mathbf{F}_{\text{RF}}$  according to the given channels  $\mathbf{H}_{\text{TR}}$ ,  $\mathbf{H}_{\text{TI}}$ , and  $\mathbf{H}_{\text{IR}}$ . That is, we focus on solving the effective channel design problem, which is formulated as

$$(P3) \quad \max_{\mathbf{W}_{\text{RF}}, \Phi, \mathbf{F}_{\text{RF}}} R_{\text{max}}(\mathbf{H}_{\text{eff}}) \quad (10a)$$

$$\text{subject to} \quad \Phi = \text{diag}([e^{j\theta_1}, \dots, e^{j\theta_M}]), \quad (10b)$$

$$\|[\mathbf{W}_{\text{RF}}]_{m,n}\| = 1/\sqrt{N_{\text{r}}}, \quad \forall m, n, \quad (10c)$$

$$\|[\mathbf{F}_{\text{RF}}]_{m,n}\| = 1/\sqrt{N_{\text{t}}}, \quad \forall m, n, \quad (10d)$$

$$\mathbf{W}_{\text{RF}}^{\text{H}} \mathbf{W}_{\text{RF}} = \mathbf{I}_{N_{\text{r}}^{\text{RF}}}, \quad \mathbf{F}_{\text{RF}}^{\text{H}} \mathbf{F}_{\text{RF}} = \mathbf{I}_{N_{\text{t}}^{\text{RF}}}. \quad (10e)$$

<sup>1</sup>From now on, we use  $R_{\text{max}}(\mathbf{H})$  to denote the maximum spectral efficiency that can be achieved under the transmit power constraint  $P_{\text{TX}}$  and channel  $\mathbf{H}$  of appropriate dimension.

Note that, given the transmit power constraint  $P_{\text{TX}}$  and noise power  $\sigma_n^2$ , the value of the objective function  $R_{\text{max}}(\mathbf{H}_{\text{eff}})$  of the problem (P3) is solely determined by  $\{|\Sigma_{\text{eff}}]_{l,l}|^2\}_{l=1}^{N_s}$ , which are necessarily the  $N_s$  largest eigenvalues of  $\mathbf{H}_{\text{eff}} \mathbf{H}_{\text{eff}}^{\text{H}}$ .

## B. IRS Reflection Pattern Design

Although the effective channel design problem (P3) developed in Section III-A involves less variables than the original problem (P1) of interest, it is still challenging to find the optimal solution of (P3) since the IRS reflection matrix  $\Phi$  directly influences the total combined channel  $\mathbf{H}_{\text{tot}}$ , which in turn determines the appropriate analog combiner  $\mathbf{W}_{\text{RF}}$  and precoder  $\mathbf{F}_{\text{RF}}$ . In order to address this difficulty, we propose in this subsection the IRS reflection pattern design that smartly leverages the structure of mmWave MIMO channels to significantly increase the spectral efficiency that  $\mathbf{H}_{\text{tot}}$  can support. After adjusting  $\Phi$  according to the proposed IRS design, we will construct  $\mathbf{W}_{\text{RF}}$  and  $\mathbf{F}_{\text{RF}}$  that successfully translate the spectral efficiency gain in  $\mathbf{H}_{\text{tot}} = \mathbf{H}_{\text{TR}} + \mathbf{H}_{\text{IR}} \Phi \mathbf{H}_{\text{TI}}$  to that in  $\mathbf{H}_{\text{eff}} = \mathbf{W}_{\text{RF}}^{\text{H}} \mathbf{H}_{\text{tot}} \mathbf{F}_{\text{RF}}$ , details of which are explained in Section III-C.

Let the SVD of  $\mathbf{H}_{\text{tot}}$  be expressed as  $\mathbf{H}_{\text{tot}} = \mathbf{U}_{\text{tot}} \Sigma_{\text{tot}} \mathbf{V}_{\text{tot}}^{\text{H}}$ . Then, similar to  $R_{\text{max}}(\mathbf{H}_{\text{eff}})$  in (9), the maximum achievable spectral efficiency  $R_{\text{max}}(\mathbf{H}_{\text{tot}})$  under  $\mathbf{H}_{\text{tot}}$  depends only on  $\{|\Sigma_{\text{tot}}]_{l,l}|^2\}_{l=1}^{N_s}$ , or equivalently the  $N_s$  largest eigenvalues of  $\mathbf{H}_{\text{tot}} \mathbf{H}_{\text{tot}}^{\text{H}}$ , for given  $P_{\text{TX}}$  and  $\sigma_n^2$ . To mathematically characterize the eigenvalues of  $\mathbf{H}_{\text{tot}} \mathbf{H}_{\text{tot}}^{\text{H}}$ , we first define the receive array response matrix  $\mathbf{A}_{\text{r}}^i$ , complex gain matrix  $\mathbf{G}_i$ , and transmit array response matrix  $\mathbf{A}_{\text{t}}^i$  for the mmWave channel  $\mathbf{H}_i$  in (3) as

$$\begin{aligned} \mathbf{A}_{\text{r}}^i &= \begin{bmatrix} \mathbf{a}_{\text{r}}(\phi_{i,0}^{\text{r}}, \theta_{i,0}^{\text{r}}) & \cdots & \mathbf{a}_{\text{r}}(\phi_{i,N_{\text{path}}^i-1}^{\text{r}}, \theta_{i,N_{\text{path}}^i-1}^{\text{r}}) \end{bmatrix}, \\ \mathbf{G}_i &= \text{diag}([\alpha_{i,0}, \dots, \alpha_{i,N_{\text{path}}^i-1}]), \\ \mathbf{A}_{\text{t}}^i &= \begin{bmatrix} \mathbf{a}_{\text{t}}(\phi_{i,0}^{\text{t}}, \theta_{i,0}^{\text{t}}) & \cdots & \mathbf{a}_{\text{t}}(\phi_{i,N_{\text{path}}^i-1}^{\text{t}}, \theta_{i,N_{\text{path}}^i-1}^{\text{t}}) \end{bmatrix}. \end{aligned} \quad (11)$$

The channel matrix  $\mathbf{H}_i$  can then be decomposed as

$$\mathbf{H}_i = \mathbf{A}_{\text{r}}^i \mathbf{G}_i (\mathbf{A}_{\text{t}}^i)^{\text{H}}, \quad (12)$$

where we assume, without loss of generality, that  $|\mathbf{G}_i]_{m,m}| \geq |\mathbf{G}_i]_{n,n}|, \forall m, n \in \{1, \dots, N_{\text{path}}^i\}$  such that  $m < n$ . We now pay particular attention to  $\mathbf{H}_{\text{TR}} \mathbf{H}_{\text{TI}}^{\text{H}}$ , which can be written as

$$\mathbf{H}_{\text{TR}} \mathbf{H}_{\text{TI}}^{\text{H}} = \mathbf{A}_{\text{r}}^{\text{TR}} \mathbf{G}_{\text{TR}} (\mathbf{A}_{\text{t}}^{\text{TR}})^{\text{H}} \mathbf{A}_{\text{t}}^{\text{TI}} \mathbf{G}_{\text{TI}}^{\text{H}} (\mathbf{A}_{\text{r}}^{\text{TI}})^{\text{H}}. \quad (13)$$

Since the AoDs of different propagation paths can be considered as continuous random variables that are independent from one another, it follows that the event  $E = \{\phi_{\text{TR},s}^{\text{t}} \neq \phi_{\text{TI},j}^{\text{t}}, \theta_{\text{TR},s}^{\text{t}} \neq \theta_{\text{TI},j}^{\text{t}}, \forall s \in \{0, \dots, N_{\text{path}}^{\text{TR}} - 1\}, \forall j \in \{0, \dots, N_{\text{path}}^{\text{TI}} - 1\}\}$  occurs with probability one [26], [29]. Then, by the asymptotic orthogonality of UPA array response vectors [30], we have

$$(\mathbf{A}_{\text{t}}^{\text{TR}})^{\text{H}} \mathbf{A}_{\text{t}}^{\text{TI}} \rightarrow \mathbf{0}_{N_{\text{path}}^{\text{TR}} \times N_{\text{path}}^{\text{TI}}}, \text{ as } N_{\text{t}} \rightarrow \infty, \quad (14)$$

which implies that each element of  $\mathbf{H}_{\text{TR}}\mathbf{H}_{\text{TI}}^{\text{H}}$  converges to 0 in the limit of large  $N_t$ . Using similar arguments, we can show that

$$\begin{aligned} \mathbf{H}_{\text{tot}}\mathbf{H}_{\text{tot}}^{\text{H}} &= \mathbf{H}_{\text{TR}}\mathbf{H}_{\text{TR}}^{\text{H}} + \mathbf{H}_{\text{TR}}\mathbf{H}_{\text{TI}}^{\text{H}}\mathbf{\Phi}\mathbf{H}_{\text{TI}}^{\text{H}}\mathbf{H}_{\text{IR}}^{\text{H}} \\ &\quad + \mathbf{H}_{\text{IR}}\mathbf{\Phi}\mathbf{H}_{\text{TI}}^{\text{H}}\mathbf{H}_{\text{TR}}^{\text{H}} + \mathbf{H}_{\text{IR}}\mathbf{\Phi}\mathbf{H}_{\text{TI}}^{\text{H}}\mathbf{H}_{\text{TI}}^{\text{H}}\mathbf{\Phi}^{\text{H}}\mathbf{H}_{\text{IR}}^{\text{H}} \\ &\rightarrow \sum_{s=0}^{N_{\text{path}}^{\text{TR}}-1} |\alpha_{\text{TR},s}|^2 \mathbf{a}_{\text{r}}(\phi_{\text{TR},s}^{\text{r}}, \theta_{\text{TR},s}^{\text{r}}) \mathbf{a}_{\text{r}}(\phi_{\text{TR},s}^{\text{r}}, \theta_{\text{TR},s}^{\text{r}})^{\text{H}} \\ &\quad + \sum_{j=0}^{N_{\text{path}}^{\text{TI}}-1} |\alpha_{\text{TI},j}|^2 \mathbf{q}_j \mathbf{q}_j^{\text{H}}, \end{aligned} \quad (15)$$

as  $N_t \rightarrow \infty$ , where  $\mathbf{q}_j = \mathbf{H}_{\text{IR}}\mathbf{\Phi}\mathbf{a}_{\text{r}}(\phi_{\text{TI},j}^{\text{r}}, \theta_{\text{TI},j}^{\text{r}})$ ,  $j \in \{0, \dots, N_{\text{path}}^{\text{TI}} - 1\}$ .

We now present the following lemma to establish the connection between the magnitude of  $\mathbf{q}_j$  and IRS reflection matrix  $\mathbf{\Phi}$ .

*Lemma 1:* For any  $j \in \{0, \dots, N_{\text{path}}^{\text{TI}} - 1\}$ ,  $\|\mathbf{q}_j\|_2^2$  satisfies

$$\|\mathbf{q}_j\|_2^2 \leq \lambda_0(\mathbf{H}_{\text{IR}}^{\text{H}}\mathbf{H}_{\text{IR}}), \quad (16)$$

where the equality holds if  $\mathbf{\Phi}\mathbf{a}_{\text{r}}(\phi_{\text{TI},j}^{\text{r}}, \theta_{\text{TI},j}^{\text{r}})$  is the eigenvector corresponding to the maximum eigenvalue  $\lambda_0(\mathbf{H}_{\text{IR}}^{\text{H}}\mathbf{H}_{\text{IR}})$  of  $\mathbf{H}_{\text{IR}}^{\text{H}}\mathbf{H}_{\text{IR}}$ , i.e.,  $\mathbf{H}_{\text{IR}}^{\text{H}}\mathbf{H}_{\text{IR}}\mathbf{\Phi}\mathbf{a}_{\text{r}}(\phi_{\text{TI},j}^{\text{r}}, \theta_{\text{TI},j}^{\text{r}}) = \lambda_0(\mathbf{H}_{\text{IR}}^{\text{H}}\mathbf{H}_{\text{IR}})\mathbf{\Phi}\mathbf{a}_{\text{r}}(\phi_{\text{TI},j}^{\text{r}}, \theta_{\text{TI},j}^{\text{r}})$ .

*Proof:* See Appendix A.  $\square$

While it is in general impossible to express the eigenvalues of  $\mathbf{H}_{\text{IR}}^{\text{H}}\mathbf{H}_{\text{IR}}$  explicitly, the following lemma describes their asymptotic characteristics.

*Lemma 2:* Let  $m \in \{0, \dots, N_{\text{path}}^{\text{IR}} - 1\}$ . Then, as  $N_r, M \rightarrow \infty$ ,

$$\mathbf{H}_{\text{IR}}^{\text{H}}\mathbf{H}_{\text{IR}}\mathbf{a}_{\text{t}}(\phi_{\text{IR},m}^{\text{l}}, \theta_{\text{IR},m}^{\text{l}}) \rightarrow |\alpha_{\text{IR},m}|^2 \mathbf{a}_{\text{t}}(\phi_{\text{IR},m}^{\text{l}}, \theta_{\text{IR},m}^{\text{l}}). \quad (17)$$

*Proof:* Fix  $m \in \{0, \dots, N_{\text{path}}^{\text{IR}} - 1\}$ . By a similar argument used to derive (14), we have

$$(\mathbf{A}_{\text{r}}^{\text{IR}})^{\text{H}}\mathbf{A}_{\text{r}}^{\text{IR}} \rightarrow \mathbf{I}_{N_{\text{path}}^{\text{IR}}}, \text{ as } N_r \rightarrow \infty,$$

$$(\mathbf{A}_{\text{t}}^{\text{IR}})^{\text{H}}\mathbf{a}_{\text{t}}(\phi_{\text{IR},m}^{\text{l}}, \theta_{\text{IR},m}^{\text{l}}) \rightarrow [\mathbf{I}_{N_{\text{path}}^{\text{IR}}}]_{:,m+1}, \text{ as } M \rightarrow \infty. \quad (18)$$

Combining (18) with  $\mathbf{H}_{\text{IR}} = \mathbf{A}_{\text{r}}^{\text{IR}}\mathbf{G}_{\text{IR}}(\mathbf{A}_{\text{t}}^{\text{IR}})^{\text{H}}$ , we obtain that

$$\mathbf{H}_{\text{IR}}^{\text{H}}\mathbf{H}_{\text{IR}}\mathbf{a}_{\text{t}}(\phi_{\text{IR},m}^{\text{l}}, \theta_{\text{IR},m}^{\text{l}}) \rightarrow \mathbf{A}_{\text{t}}^{\text{IR}}\mathbf{G}_{\text{IR}}^{\text{H}}\mathbf{G}_{\text{IR}}[\mathbf{I}_{N_{\text{path}}^{\text{IR}}}]_{:,m+1}, \quad (19)$$

as  $N_r, M \rightarrow \infty$ . Since (19) is equivalent to (17), the proof of Lemma 2 is complete.  $\square$

With the aid of Lemmas 1 and 2, we now show in the following proposition that the IRS reflection matrix  $\mathbf{\Phi}$  that asymptotically maximizes  $\|\mathbf{q}_j\|_2^2$  can be obtained in closed-form.

*Proposition 1:* Let  $j \in \{0, \dots, N_{\text{path}}^{\text{TI}} - 1\}$  and define the vector  $\mathbf{v} \in \mathbb{C}^{M \times 1}$  that satisfies  $\mathbf{\Phi} = \text{diag}(\mathbf{v})$ . Then, when  $\mathbf{v} = M \text{diag}(\mathbf{a}_{\text{r}}(\phi_{\text{TI},j}^{\text{r}}, \theta_{\text{TI},j}^{\text{r}})^{\text{H}})\mathbf{a}_{\text{t}}(\phi_{\text{IR},0}^{\text{l}}, \theta_{\text{IR},0}^{\text{l}})$ , it holds that

$$\|\mathbf{q}_j\|_2^2 \rightarrow \lambda_0(\mathbf{H}_{\text{IR}}^{\text{H}}\mathbf{H}_{\text{IR}}), \text{ as } N_r, M \rightarrow \infty. \quad (20)$$

*Proof:* Set  $j \in \{0, \dots, N_{\text{path}}^{\text{TI}} - 1\}$  and  $\mathbf{v} = M \text{diag}(\mathbf{a}_{\text{r}}(\phi_{\text{TI},j}^{\text{r}}, \theta_{\text{TI},j}^{\text{r}})^{\text{H}})\mathbf{a}_{\text{t}}(\phi_{\text{IR},0}^{\text{l}}, \theta_{\text{IR},0}^{\text{l}})$ . We can then write

$$\begin{aligned} \mathbf{\Phi}\mathbf{a}_{\text{r}}(\phi_{\text{TI},j}^{\text{r}}, \theta_{\text{TI},j}^{\text{r}}) &= \text{diag}(\mathbf{a}_{\text{r}}(\phi_{\text{TI},j}^{\text{r}}, \theta_{\text{TI},j}^{\text{r}}))\mathbf{v} \\ &= \mathbf{a}_{\text{t}}(\phi_{\text{IR},0}^{\text{l}}, \theta_{\text{IR},0}^{\text{l}}). \end{aligned} \quad (21)$$

From (17) in Lemma 2, we have

$$\mathbf{H}_{\text{IR}}^{\text{H}}\mathbf{H}_{\text{IR}}\mathbf{a}_{\text{t}}(\phi_{\text{IR},0}^{\text{l}}, \theta_{\text{IR},0}^{\text{l}}) \rightarrow |\alpha_{\text{IR},0}|^2 \mathbf{a}_{\text{t}}(\phi_{\text{IR},0}^{\text{l}}, \theta_{\text{IR},0}^{\text{l}}), \quad (22)$$

as  $N_r, M \rightarrow \infty$ . Since Lemma 1 states that  $\|\mathbf{q}_j\|_2^2 = \lambda_0(\mathbf{H}_{\text{IR}}^{\text{H}}\mathbf{H}_{\text{IR}})$  when  $\mathbf{\Phi}\mathbf{a}_{\text{r}}(\phi_{\text{TI},j}^{\text{r}}, \theta_{\text{TI},j}^{\text{r}})$  is the eigenvector of  $\mathbf{H}_{\text{IR}}^{\text{H}}\mathbf{H}_{\text{IR}}$  associated with  $\lambda_0(\mathbf{H}_{\text{IR}}^{\text{H}}\mathbf{H}_{\text{IR}})$ , we can prove Proposition 1 by showing that  $|\alpha_{\text{IR},0}|^2$  asymptotically becomes the maximum eigenvalue of  $\mathbf{H}_{\text{IR}}^{\text{H}}\mathbf{H}_{\text{IR}}$  in the limit of large  $N_r$  and  $M$ . Noting that  $\mathbf{H}_{\text{IR}}^{\text{H}} = \mathbf{A}_{\text{t}}^{\text{IR}}\mathbf{G}_{\text{IR}}^{\text{H}}(\mathbf{A}_{\text{r}}^{\text{IR}})^{\text{H}}$ , we have

$$\text{rank}(\mathbf{H}_{\text{IR}}^{\text{H}}\mathbf{H}_{\text{IR}}) \leq \text{rank}(\mathbf{A}_{\text{t}}^{\text{IR}}) \leq \min(M, N_{\text{path}}^{\text{IR}}). \quad (23)$$

The inequality in (23) implies that  $\mathbf{H}_{\text{IR}}^{\text{H}}\mathbf{H}_{\text{IR}}$  can have at most  $N_{\text{path}}^{\text{IR}}$  nonzero eigenvalues, counting multiplicities, for sufficiently large  $M$  such that  $M \geq N_{\text{path}}^{\text{IR}}$ . In fact, Lemma 2 states that  $|\alpha_{\text{IR},m}|^2$  asymptotically becomes the eigenvalue of  $\mathbf{H}_{\text{IR}}^{\text{H}}\mathbf{H}_{\text{IR}}$  for each  $m \in \{0, \dots, N_{\text{path}}^{\text{IR}} - 1\}$ , i.e., the number of nonzero eigenvalues of  $\mathbf{H}_{\text{IR}}^{\text{H}}\mathbf{H}_{\text{IR}}$  approaches  $N_{\text{path}}^{\text{IR}}$  as  $N_r, M \rightarrow \infty$ . Since  $|\alpha_{\text{IR},0}|^2 \geq |\alpha_{\text{IR},m}|^2$  for each  $m$ , we have

$$\lambda_0(\mathbf{H}_{\text{IR}}^{\text{H}}\mathbf{H}_{\text{IR}}) \rightarrow |\alpha_{\text{IR},0}|^2, \text{ as } N_r, M \rightarrow \infty. \quad (24)$$

This completes the proof of Proposition 1.  $\square$

To examine how setting  $\mathbf{\Phi}$  as described in Proposition 1 modifies the value of  $\|\mathbf{q}_p\|_2^2$ ,  $p \in \{0, \dots, N_{\text{path}}^{\text{TI}} - 1\} \setminus \{j\}$ , we first express  $\mathbf{q}_p$  as

$$\begin{aligned} \mathbf{q}_p &= \mathbf{H}_{\text{IR}}\mathbf{\Phi}\mathbf{a}_{\text{r}}(\phi_{\text{TI},p}^{\text{r}}, \theta_{\text{TI},p}^{\text{r}}) \\ &= \mathbf{A}_{\text{r}}^{\text{IR}}\mathbf{G}_{\text{IR}}(\mathbf{A}_{\text{t}}^{\text{IR}})^{\text{H}}\text{diag}(\mathbf{a}_{\text{r}}(\phi_{\text{TI},p}^{\text{r}}, \theta_{\text{TI},p}^{\text{r}}))\mathbf{v}. \end{aligned} \quad (25)$$

By direct computation, we can express the  $(m+1)$ -th element of  $(\mathbf{A}_{\text{t}}^{\text{IR}})^{\text{H}}\text{diag}(\mathbf{a}_{\text{r}}(\phi_{\text{TI},p}^{\text{r}}, \theta_{\text{TI},p}^{\text{r}}))\mathbf{v}$  as

$$\begin{aligned} [(\mathbf{A}_{\text{t}}^{\text{IR}})^{\text{H}}\text{diag}(\mathbf{a}_{\text{r}}(\phi_{\text{TI},p}^{\text{r}}, \theta_{\text{TI},p}^{\text{r}}))\mathbf{v}]_{m+1} \\ = \mathbf{a}(f_{m,p}, g_{m,p})^{\text{H}}\mathbf{a}(f_{0,j}, g_{0,j}), \end{aligned} \quad (26)$$

where  $m \in \{0, \dots, N_{\text{path}}^{\text{IR}} - 1\}$ ,  $f_{m,p} = \sin(\phi_{\text{IR},m}^{\text{l}})\sin(\theta_{\text{IR},m}^{\text{l}}) - \sin(\phi_{\text{TI},p}^{\text{r}})\sin(\theta_{\text{TI},p}^{\text{r}})$ , and  $g_{m,p} = \cos(\theta_{\text{IR},m}^{\text{l}}) - \cos(\theta_{\text{TI},p}^{\text{r}})$ . The vector  $\mathbf{a}(f, g) \in \mathbb{C}^{M \times 1}$  is expressed as

$$\begin{aligned} \mathbf{a}(f, g) &= \frac{1}{\sqrt{M}} \left[ 1, \dots, e^{j\frac{2\pi d}{\lambda}(m_h f + m_v g)}, \right. \\ &\quad \left. \dots, e^{j\frac{2\pi d}{\lambda}((M^h - 1)f + (M^v - 1)g)} \right]^{\text{T}}. \end{aligned} \quad (27)$$

Here,  $0 \leq m_h < M^h$  and  $0 \leq m_v < M^v$  each denote the horizontal and vertical indices for the IRS elements, where  $M = M^h M^v$ . Since the vector  $\mathbf{a}(f, g)$  has the same structure as an  $M \times 1$  UPA array response vector, it follows that each element of  $(\mathbf{A}_{\text{t}}^{\text{IR}})^{\text{H}}\text{diag}(\mathbf{a}_{\text{r}}(\phi_{\text{TI},p}^{\text{r}}, \theta_{\text{TI},p}^{\text{r}}))\mathbf{v}$  tends to zero as  $M \rightarrow \infty$ . We can thus conclude from (25) that

$$\|\mathbf{q}_p\|_2^2 \rightarrow 0, \text{ as } M \rightarrow \infty, \quad (28)$$

for any  $p \in \{0, \dots, N_{\text{path}}^{\text{TI}} - 1\} \setminus \{j\}$ .

We now explain in the following proposition how the eigenvalues of  $\mathbf{H}_{\text{tot}}\mathbf{H}_{\text{tot}}^{\text{H}}$  asymptotically behave when  $\Phi$  is set as described in Proposition 1.

*Proposition 2:* Let  $j^* \in \{0, \dots, N_{\text{path}}^{\text{TI}} - 1\}$  and  $s \in \{0, \dots, N_{\text{path}}^{\text{TR}} - 1\}$ . When  $\Phi = \text{diag}(\mathbf{v})$ ,  $\mathbf{v} = M \text{diag}(\mathbf{a}_r(\phi_{\text{TI},j^*}^r, \theta_{\text{TI},j^*}^r)^{\text{H}}) \mathbf{a}_t(\phi_{\text{IR},0}^t, \theta_{\text{IR},0}^t)$ , it holds that

$$\mathbf{H}_{\text{tot}}\mathbf{H}_{\text{tot}}^{\text{H}} \mathbf{a}_r(\phi_{\text{IR},0}^r, \theta_{\text{IR},0}^r) \rightarrow |\alpha_{\text{TI},j^*}|^2 |\alpha_{\text{IR},0}|^2 \mathbf{a}_r(\phi_{\text{IR},0}^r, \theta_{\text{IR},0}^r), \quad (29)$$

$$\mathbf{H}_{\text{tot}}\mathbf{H}_{\text{tot}}^{\text{H}} \mathbf{a}_r(\phi_{\text{TR},s}^r, \theta_{\text{TR},s}^r) \rightarrow |\alpha_{\text{TR},s}|^2 \mathbf{a}_r(\phi_{\text{TR},s}^r, \theta_{\text{TR},s}^r), \quad (30)$$

as  $N_t, N_r, M \rightarrow \infty$ .

*Proof:* Set  $\mathbf{v} = M \text{diag}(\mathbf{a}_r(\phi_{\text{TI},j^*}^r, \theta_{\text{TI},j^*}^r)^{\text{H}}) \mathbf{a}_t(\phi_{\text{IR},0}^t, \theta_{\text{IR},0}^t)$ ,  $j^* \in \{0, \dots, N_{\text{path}}^{\text{TI}} - 1\}$ . According to (12), (18), and (21), we can express  $\mathbf{q}_{j^*}$  as

$$\begin{aligned} \mathbf{q}_{j^*} &= \mathbf{A}_r^{\text{IR}} \mathbf{G}_{\text{IR}} (\mathbf{A}_t^{\text{IR}})^{\text{H}} \mathbf{a}_t(\phi_{\text{IR},0}^t, \theta_{\text{IR},0}^t) \\ &\rightarrow \alpha_{\text{IR},0} \mathbf{a}_r(\phi_{\text{IR},0}^r, \theta_{\text{IR},0}^r), \text{ as } M \rightarrow \infty. \end{aligned} \quad (31)$$

Combining (28) and (31) with (15), we have

$$\begin{aligned} \mathbf{H}_{\text{tot}}\mathbf{H}_{\text{tot}}^{\text{H}} &\rightarrow \sum_{s=0}^{N_{\text{path}}^{\text{TR}}-1} |\alpha_{\text{TR},s}|^2 \mathbf{a}_r(\phi_{\text{TR},s}^r, \theta_{\text{TR},s}^r) \mathbf{a}_r(\phi_{\text{TR},s}^r, \theta_{\text{TR},s}^r)^{\text{H}} \\ &+ |\alpha_{\text{TI},j^*}|^2 |\alpha_{\text{IR},0}|^2 \mathbf{a}_r(\phi_{\text{IR},0}^r, \theta_{\text{IR},0}^r) \mathbf{a}_r(\phi_{\text{IR},0}^r, \theta_{\text{IR},0}^r)^{\text{H}}, \end{aligned} \quad (32)$$

as  $N_t, M \rightarrow \infty$ . Also, it holds for each  $s \in \{0, \dots, N_{\text{path}}^{\text{TR}} - 1\}$  that

$$\mathbf{a}_r(\phi_{\text{TR},s}^r, \theta_{\text{TR},s}^r)^{\text{H}} \mathbf{a}_r(\phi_{\text{IR},0}^r, \theta_{\text{IR},0}^r) \rightarrow 0, \text{ as } N_r \rightarrow \infty, \quad (33)$$

since the event  $T_s = \{\phi_{\text{TR},s}^r \neq \phi_{\text{IR},0}^r, \theta_{\text{TR},s}^r \neq \theta_{\text{IR},0}^r\}$  occurs with probability one. It then follows from (32) and (33) that

$$\begin{aligned} \mathbf{H}_{\text{tot}}\mathbf{H}_{\text{tot}}^{\text{H}} \mathbf{a}_r(\phi_{\text{IR},0}^r, \theta_{\text{IR},0}^r) &\rightarrow |\alpha_{\text{TI},j^*}|^2 |\alpha_{\text{IR},0}|^2 \mathbf{a}_r(\phi_{\text{IR},0}^r, \theta_{\text{IR},0}^r), \\ &\text{as } N_t, N_r, M \rightarrow \infty, \end{aligned} \quad (34)$$

which finishes the proof of (29). To verify (30), we first note that

$$(\mathbf{A}_r^{\text{TR}})^{\text{H}} \mathbf{A}_r^{\text{TR}} \rightarrow \mathbf{I}_{N_{\text{path}}^{\text{TR}}}, \text{ as } N_r \rightarrow \infty. \quad (35)$$

By the results in (32), (33), and (35), we have for any  $s \in \{0, \dots, N_{\text{path}}^{\text{TR}} - 1\}$  that

$$\mathbf{H}_{\text{tot}}\mathbf{H}_{\text{tot}}^{\text{H}} \mathbf{a}_r(\phi_{\text{TR},s}^r, \theta_{\text{TR},s}^r) \rightarrow |\alpha_{\text{TR},s}|^2 \mathbf{a}_r(\phi_{\text{TR},s}^r, \theta_{\text{TR},s}^r), \quad (36)$$

as  $N_t, N_r, M \rightarrow \infty$ , which completes the proof of (30).  $\square$

According to Proposition 2,  $|\alpha_{\text{TI},j^*}|^2 |\alpha_{\text{IR},0}|^2$  and  $\{|\alpha_{\text{TR},s}|^2\}_{s=0}^{N_{\text{path}}^{\text{TR}}-1}$  are the asymptotic eigenvalues of  $\mathbf{H}_{\text{tot}}\mathbf{H}_{\text{tot}}^{\text{H}}$  when  $\mathbf{v} = M \text{diag}(\mathbf{a}_r(\phi_{\text{TI},j^*}^r, \theta_{\text{TI},j^*}^r)^{\text{H}}) \mathbf{a}_t(\phi_{\text{IR},0}^t, \theta_{\text{IR},0}^t)$ . As  $R_{\text{max}}(\mathbf{H}_{\text{tot}})$  monotonically increases with the eigenvalues of  $\mathbf{H}_{\text{tot}}\mathbf{H}_{\text{tot}}^{\text{H}}$  for given  $P_{\text{TX}}$  and  $\sigma_n^2$ , we set the IRS reflection matrix as  $\Phi^* = \text{diag}(\mathbf{v}^*)$ , where

$$\mathbf{v}^* = M \text{diag}(\mathbf{a}_r(\phi_{\text{TI},0}^r, \theta_{\text{TI},0}^r)^{\text{H}}) \mathbf{a}_t(\phi_{\text{IR},0}^t, \theta_{\text{IR},0}^t), \quad (37)$$

so that  $|\alpha_{\text{TI},0}|^2 |\alpha_{\text{IR},0}|^2$  becomes the eigenvalue of  $\mathbf{H}_{\text{tot}}\mathbf{H}_{\text{tot}}^{\text{H}}$  in the limit of large  $N_t, N_r$  and  $M$ .

To investigate how the structure of mmWave MIMO channels is adjusted by the proposed IRS reflection pattern design, we first express the reflected channel  $\mathbf{H}_{\text{IR}}\Phi^*\mathbf{H}_{\text{TI}}$  as

$$\mathbf{H}_{\text{IR}}\Phi^*\mathbf{H}_{\text{TI}} = \mathbf{A}_r^{\text{IR}} \mathbf{G}_{\text{IR}} (\mathbf{A}_t^{\text{IR}})^{\text{H}} \Phi^* \mathbf{A}_r^{\text{TI}} \mathbf{G}_{\text{TI}} (\mathbf{A}_t^{\text{TI}})^{\text{H}}. \quad (38)$$

Using the expression in (27), we can write the element in the  $(m+1)$ -th row and  $(j+1)$ -th column of  $\mathbf{C} = (\mathbf{A}_t^{\text{IR}})^{\text{H}} \Phi^* \mathbf{A}_r^{\text{TI}}$  as

$$[\mathbf{C}]_{m+1,j+1} = \begin{cases} \mathbf{a}_t(\phi_{\text{IR},m}^t, \theta_{\text{IR},m}^t)^{\text{H}} \mathbf{a}_t(\phi_{\text{IR},0}^t, \theta_{\text{IR},0}^t) & \text{if } j = 0, \\ \mathbf{a}(f_{m,j}, g_{m,j})^{\text{H}} \mathbf{a}(f_{0,0}, g_{0,0}) & \text{if } j \neq 0, \end{cases} \quad (39)$$

for each  $m \in \{0, \dots, N_{\text{path}}^{\text{IR}} - 1\}$  and  $j \in \{0, \dots, N_{\text{path}}^{\text{TI}} - 1\}$ . It is evident from (39) that the asymptotic behavior of  $[\mathbf{C}]_{m+1,j+1}$  can be characterized as

$$[\mathbf{C}]_{m+1,j+1} \rightarrow \delta_{m0} \delta_{j0}, \text{ as } M \rightarrow \infty, \quad (40)$$

where  $\delta_{xy}$  is the Kronecker delta function that takes the value of 1 if and only if  $x = y$ . As a result, the adjusted total channel  $\mathbf{H}_{\text{tot}}^* = \mathbf{H}_{\text{TR}} + \mathbf{H}_{\text{IR}}\Phi^*\mathbf{H}_{\text{TI}}$  satisfies

$$\begin{aligned} \mathbf{H}_{\text{tot}}^* &\rightarrow \sum_{s=0}^{N_{\text{path}}^{\text{TR}}-1} \alpha_{\text{TR},s} \mathbf{a}_r(\phi_{\text{TR},s}^r, \theta_{\text{TR},s}^r) \mathbf{a}_t(\phi_{\text{TR},s}^t, \theta_{\text{TR},s}^t)^{\text{H}} \\ &+ \alpha_{\text{TI},0} \alpha_{\text{IR},0} \mathbf{a}_r(\phi_{\text{IR},0}^r, \theta_{\text{IR},0}^r) \mathbf{a}_t(\phi_{\text{TI},0}^t, \theta_{\text{TI},0}^t)^{\text{H}}, \end{aligned} \quad (41)$$

as  $M \rightarrow \infty$ . It can thus be concluded that, by asymptotically maximizing the eigenvalue associated with the dominant transmit and receive path pair at the IRS, the proposed IRS design successfully establishes a strong communication link between the TX and RX. Also, since  $\alpha_{\text{TI},0}$  and  $\alpha_{\text{IR},0}$  are independent, we have

$$\mathbb{E}[|\alpha_{\text{TI},0}|^2 |\alpha_{\text{IR},0}|^2] \geq M^2 c, \quad (42)$$

where  $c = N_t N_r 10^{-0.1(PL(d_{\text{TI}}) + PL(d_{\text{IR}}))} / N_{\text{path}}^{\text{TI}} N_{\text{path}}^{\text{IR}}$ . The inequality in (42) shows that, for a fixed value of  $c$ , the average magnitude of the asymptotic eigenvalue  $|\alpha_{\text{TI},0}|^2 |\alpha_{\text{IR},0}|^2$  of  $\mathbf{H}_{\text{tot}}^* (\mathbf{H}_{\text{tot}}^*)^{\text{H}}$  scales at least quadratically with  $M$ . This suggests that the proposed design will offer significant increases in spectral efficiency for IRS-aided mmWave MIMO systems, where the IRS passive elements are expected to be deployed in large numbers thanks to their low costs and hardware simplicity [17], [19].

### C. Analog Beamformer Design

In this subsection, we propose the analog beamformer design that leverages the structure of the favorably adjusted total channel  $\mathbf{H}_{\text{tot}}^* = \mathbf{H}_{\text{TR}} + \mathbf{H}_{\text{IR}}\Phi^*\mathbf{H}_{\text{TI}}$ . Specifically, we construct the analog precoder  $\mathbf{F}_{\text{RF}}$  and combiner  $\mathbf{W}_{\text{RF}}$  so that the effective channel  $\mathbf{W}_{\text{RF}}^{\text{H}} \mathbf{H}_{\text{tot}}^* \mathbf{F}_{\text{RF}}$  can asymptotically support the maximum spectral efficiency  $R_{\text{max}}(\mathbf{H}_{\text{tot}}^*)$  achievable with fully-digital beamforming.

With the IRS reflection pattern designed according to Section III-B, i.e.,  $\Phi = \Phi^*$ , the effective channel design problem (P3) reduces to

$$(P4) \quad \max_{\mathbf{W}_{\text{RF}}, \mathbf{F}_{\text{RF}}} R_{\text{max}}(\mathbf{W}_{\text{RF}}^{\text{H}} \mathbf{H}_{\text{tot}}^* \mathbf{F}_{\text{RF}}) \quad (43a)$$

$$\text{subject to} \quad |[\mathbf{W}_{\text{RF}}]_{m,n}| = 1/\sqrt{N_t}, \forall m, n, \quad (43b)$$

$$|[\mathbf{F}_{\text{RF}}]_{m,n}| = 1/\sqrt{N_t}, \forall m, n, \quad (43c)$$

$$\mathbf{W}_{\text{RF}}^{\text{H}} \mathbf{W}_{\text{RF}} = \mathbf{I}_{N_r^{\text{RF}}}, \mathbf{F}_{\text{RF}}^{\text{H}} \mathbf{F}_{\text{RF}} = \mathbf{I}_{N_t^{\text{RF}}}. \quad (43d)$$

Removing the constant modulus constraints (43b), (43c) of the problem (P4), we can formulate the relaxed problem (P4') as

$$(P4') \quad \max_{\mathbf{W}_{\text{RF}}, \mathbf{F}_{\text{RF}}} R_{\text{max}}(\mathbf{W}_{\text{RF}}^{\text{H}} \mathbf{H}_{\text{tot}}^* \mathbf{F}_{\text{RF}}) \quad (44a)$$

$$\text{subject to} \quad \mathbf{W}_{\text{RF}}^{\text{H}} \mathbf{W}_{\text{RF}} = \mathbf{I}_{N_r^{\text{RF}}}, \mathbf{F}_{\text{RF}}^{\text{H}} \mathbf{F}_{\text{RF}} = \mathbf{I}_{N_t^{\text{RF}}}. \quad (44b)$$

With the SVD of  $\mathbf{H}_{\text{tot}}^*$  expressed as  $\mathbf{H}_{\text{tot}}^* = \mathbf{U}_{\text{tot}}^* \boldsymbol{\Sigma}_{\text{tot}}^* (\mathbf{V}_{\text{tot}}^*)^{\text{H}}$ , it is possible to explicitly obtain the optimal solution of (P4'), as described in the following proposition.

*Proposition 3:* Let  $\{\mathbf{W}_{\text{RF}}, \mathbf{F}_{\text{RF}}\}$  be a feasible solution to the problem (P4'). Then, it holds that

$$R_{\text{max}}(\mathbf{W}_{\text{RF}}^{\text{H}} \mathbf{H}_{\text{tot}}^* \mathbf{F}_{\text{RF}}) \leq R_{\text{max}}(\mathbf{H}_{\text{tot}}^*), \quad (45)$$

where the equality holds if  $\mathbf{W}_{\text{RF}} = [\mathbf{U}_{\text{tot}}^*]_{:,1:N_r^{\text{RF}}}$  and  $\mathbf{F}_{\text{RF}} = [\mathbf{V}_{\text{tot}}^*]_{:,1:N_t^{\text{RF}}}$ . That is,  $\{\hat{\mathbf{W}}_{\text{RF}}^* = [\mathbf{U}_{\text{tot}}^*]_{:,1:N_r^{\text{RF}}}, \hat{\mathbf{F}}_{\text{RF}}^* = [\mathbf{V}_{\text{tot}}^*]_{:,1:N_t^{\text{RF}}}\}$  is optimal for the problem (P4').

*Proof:* Suppose there exists a feasible solution  $\{\mathbf{W}_{\text{RF}}, \mathbf{F}_{\text{RF}}\}$  of (P4') such that  $R_{\text{max}}(\mathbf{W}_{\text{RF}}^{\text{H}} \mathbf{H}_{\text{tot}}^* \mathbf{F}_{\text{RF}}) > R_{\text{max}}(\mathbf{H}_{\text{tot}}^*)$ . Also, let  $\{\hat{\mathbf{W}}_{\text{BB}}^*, \hat{\mathbf{F}}_{\text{BB}}^*\}$  denote the optimal solution of (P2), with  $\mathbf{H}_{\text{eff}}$  set as  $\mathbf{H}_{\text{eff}} = \mathbf{W}_{\text{RF}}^{\text{H}} \mathbf{H}_{\text{tot}}^* \mathbf{F}_{\text{RF}}$ . Then, the spectral efficiency equal to  $R_{\text{max}}(\mathbf{W}_{\text{RF}}^{\text{H}} \mathbf{H}_{\text{tot}}^* \mathbf{F}_{\text{RF}})$  can be attained under  $\mathbf{H}_{\text{tot}}^*$  by using the hybrid combiner  $\mathbf{W}_{\text{RF}} \hat{\mathbf{W}}_{\text{BB}}^*$  and precoder  $\mathbf{F}_{\text{RF}} \hat{\mathbf{F}}_{\text{BB}}^*$ . This contradicts the definition of  $R_{\text{max}}(\mathbf{H}_{\text{tot}}^*)$  and the proof of the inequality in (45) is complete.

We now verify the optimality of  $\{\hat{\mathbf{W}}_{\text{RF}}^*, \hat{\mathbf{F}}_{\text{RF}}^*\}$  for the problem (P4') by showing that  $R_{\text{max}}(\hat{\mathbf{H}}_{\text{eff}}^*) = R_{\text{max}}(\mathbf{H}_{\text{tot}}^*)$ , where  $\hat{\mathbf{H}}_{\text{eff}}^* = (\hat{\mathbf{W}}_{\text{RF}}^*)^{\text{H}} \mathbf{H}_{\text{tot}}^* \hat{\mathbf{F}}_{\text{RF}}^*$ . Direct computation reveals that  $\hat{\mathbf{H}}_{\text{eff}}^* (\hat{\mathbf{H}}_{\text{eff}}^*)^{\text{H}}$  is the diagonal matrix that satisfies

$$[\hat{\mathbf{H}}_{\text{eff}}^* (\hat{\mathbf{H}}_{\text{eff}}^*)^{\text{H}}]_{n,n} = \begin{cases} |[\boldsymbol{\Sigma}_{\text{tot}}^*]_{n,n}|^2 & \text{if } 1 \leq n \leq N_{\text{min}}^{\text{RF}}, \\ 0 & \text{otherwise,} \end{cases} \quad (46)$$

where  $N_{\text{min}}^{\text{RF}} = \min(N_r^{\text{RF}}, N_t^{\text{RF}})$ . Since  $N_s \leq N_{\text{min}}^{\text{RF}}$ , the  $N_s$  largest eigenvalues of  $\hat{\mathbf{H}}_{\text{eff}}^* (\hat{\mathbf{H}}_{\text{eff}}^*)^{\text{H}}$  coincide with those of  $\mathbf{H}_{\text{tot}}^* (\mathbf{H}_{\text{tot}}^*)^{\text{H}}$ , which finishes the proof of Proposition 3.  $\square$

To develop the analog beamformer design that provides an asymptotically optimal solution of (P4), we will now examine the asymptotic property of  $\hat{\mathbf{W}}_{\text{RF}}^*$  and  $\hat{\mathbf{F}}_{\text{RF}}^*$ . Let us first focus on  $\hat{\mathbf{W}}_{\text{RF}}^* = [\mathbf{U}_{\text{tot}}^*]_{:,1:N_r^{\text{RF}}}$ , whose column vectors are necessarily the eigenvectors of  $\mathbf{H}_{\text{tot}}^* (\mathbf{H}_{\text{tot}}^*)^{\text{H}}$ . The result in (32) indicates that  $\text{rank}(\mathbf{H}_{\text{tot}}^* (\mathbf{H}_{\text{tot}}^*)^{\text{H}})$ , or equivalently the number of nonzero eigenvalues of  $\mathbf{H}_{\text{tot}}^* (\mathbf{H}_{\text{tot}}^*)^{\text{H}}$  counting multiplicities, approaches  $N_{\text{path}}^{\text{TR}} + 1$  as  $N_t, N_r, M \rightarrow \infty$ . Since Proposition 2 states that  $\{\mathbf{a}_r(\phi_{\text{TR},s}^{\text{TR}}, \theta_{\text{TR},s}^{\text{TR}})\}_{s=0}^{N_{\text{path}}^{\text{TR}}-1}$  and  $\mathbf{a}_r(\phi_{\text{IR},0}^{\text{TR}}, \theta_{\text{IR},0}^{\text{TR}})$  asymptotically become the  $N_{\text{path}}^{\text{TR}} + 1$  eigenvectors associated with the nonzero eigenvalues of  $\mathbf{H}_{\text{tot}}^* (\mathbf{H}_{\text{tot}}^*)^{\text{H}}$ , we can conclude that, as  $N_t, N_r, M \rightarrow \infty$ , each of the eigenvectors that correspond to the nonzero eigenvalues of  $\mathbf{H}_{\text{tot}}^* (\mathbf{H}_{\text{tot}}^*)^{\text{H}}$  and are in the columns of  $\hat{\mathbf{W}}_{\text{RF}}^*$  can be expressed as a scalar multiple of one of the column vectors of  $\hat{\mathbf{U}}_{\text{tot}}^* = [\mathbf{A}_r^{\text{TR}} \quad \mathbf{a}_r(\phi_{\text{IR},0}^{\text{TR}}, \theta_{\text{IR},0}^{\text{TR}})] \in \mathbb{C}^{N_r \times (N_{\text{path}}^{\text{TR}} + 1)}$ . By similar argument, we can also show that each eigenvector that is associated with a nonzero eigenvalue of  $(\mathbf{H}_{\text{tot}}^*)^{\text{H}} \mathbf{H}_{\text{tot}}^*$  and is in one of the columns of  $\hat{\mathbf{F}}_{\text{RF}}^* = [\mathbf{V}_{\text{tot}}^*]_{:,1:N_t^{\text{RF}}}$  approaches a scalar multiple of one of the column

vectors of  $\hat{\mathbf{V}}_{\text{tot}}^* = [\mathbf{A}_t^{\text{TR}} \quad \mathbf{a}_t(\phi_{\text{TI},0}^{\text{I}}, \theta_{\text{TI},0}^{\text{I}})] \in \mathbb{C}^{N_t \times (N_{\text{path}}^{\text{TR}} + 1)}$  in the limit of large  $N_t, N_r$ , and  $M$ .

Motivated by the above formulation, we now construct the analog precoder  $\mathbf{F}_{\text{RF}}^*$  and combiner  $\mathbf{W}_{\text{RF}}^*$  that are highly effective in IRS-aided mmWave MIMO systems with a large number of antennas and IRS elements. First, among the column vectors  $\mathbf{A}_t = [\mathbf{A}_t^{\text{TR}} \quad \mathbf{A}_t^{\text{TI}}]$ , we select the  $N_t^{\text{RF}}$  vectors that have the  $N_t^{\text{RF}}$  largest quadratic norm  $\|\cdot\|_{(\mathbf{H}_{\text{tot}}^*)^{\text{H}} \mathbf{H}_{\text{tot}}^*}$ , which is defined for a vector  $\mathbf{x} \in \mathbb{C}^{N_t \times 1}$  as

$$\|\mathbf{x}\|_{(\mathbf{H}_{\text{tot}}^*)^{\text{H}} \mathbf{H}_{\text{tot}}^*} = |\mathbf{x}^{\text{H}} (\mathbf{H}_{\text{tot}}^*)^{\text{H}} \mathbf{H}_{\text{tot}}^* \mathbf{x}|^{1/2} = \|\mathbf{H}_{\text{tot}}^* \mathbf{x}\|_2. \quad (47)$$

We then set these  $N_t^{\text{RF}}$  selected vectors as the column vectors of  $\mathbf{F}_{\text{RF}}^*$ . Similarly, the column vectors of the analog combiner  $\mathbf{W}_{\text{RF}}^*$  are set as the  $N_r^{\text{RF}}$  column vectors of  $\mathbf{A}_r = [\mathbf{A}_r^{\text{TR}} \quad \mathbf{A}_r^{\text{IR}}]$  with the  $N_r^{\text{RF}}$  largest quadratic norm  $\|\cdot\|_{\mathbf{H}_{\text{tot}}^* (\mathbf{H}_{\text{tot}}^*)^{\text{H}}}$ , which is defined for a vector  $\mathbf{y} \in \mathbb{C}^{N_r \times 1}$  as

$$\|\mathbf{y}\|_{\mathbf{H}_{\text{tot}}^* (\mathbf{H}_{\text{tot}}^*)^{\text{H}}} = |\mathbf{y}^{\text{H}} \mathbf{H}_{\text{tot}}^* (\mathbf{H}_{\text{tot}}^*)^{\text{H}} \mathbf{y}|^{1/2} = \|(\mathbf{H}_{\text{tot}}^*)^{\text{H}} \mathbf{y}\|_2. \quad (48)$$

According to Proposition 3 and the asymptotic property of  $\hat{\mathbf{W}}_{\text{RF}}^*$  and  $\hat{\mathbf{F}}_{\text{RF}}^*$  discussed in the preceding paragraph, we see that the effective channel  $\mathbf{H}_{\text{eff}}^* = (\mathbf{W}_{\text{RF}}^*)^{\text{H}} \mathbf{H}_{\text{tot}}^* \mathbf{F}_{\text{RF}}^*$  satisfies

$$R_{\text{max}}(\mathbf{H}_{\text{eff}}^*) \rightarrow R_{\text{max}}(\hat{\mathbf{H}}_{\text{eff}}^*) = R_{\text{max}}(\mathbf{H}_{\text{tot}}^*), \quad (49)$$

as  $N_t, N_r, M \rightarrow \infty$ . Therefore, even with limited number of RF chains, the proposed analog beamformer design successfully constructs the effective channel  $\mathbf{H}_{\text{eff}}^*$  whose maximum supportable spectral efficiency  $R_{\text{max}}(\mathbf{H}_{\text{eff}}^*)$  is very close to  $R_{\text{max}}(\mathbf{H}_{\text{tot}}^*)$  in the systems of interest, thereby harvesting the substantial spectral efficiency gain provided by the IRS reflection pattern design in Section III-B.

#### D. Baseband Beamformer Design

In the previous two subsections, we described how to design the IRS reflection pattern and analog beamformer for the channel matrices  $\mathbf{H}_{\text{TR}}, \mathbf{H}_{\text{TI}}$  and  $\mathbf{H}_{\text{IR}}$ . In this subsection, we propose the design of the baseband combiner and precoder that are nearly optimal for the effective channel  $\mathbf{H}_{\text{eff}}^* = (\mathbf{W}_{\text{RF}}^*)^{\text{H}} \mathbf{H}_{\text{tot}}^* \mathbf{F}_{\text{RF}}^*$ . As explained in Section III-A, when  $(\mathbf{W}_{\text{RF}}^*)^{\text{H}} \mathbf{W}_{\text{RF}}^* = \mathbf{I}_{N_r^{\text{RF}}}$  and  $(\mathbf{F}_{\text{RF}}^*)^{\text{H}} \mathbf{F}_{\text{RF}}^* = \mathbf{I}_{N_t^{\text{RF}}}$  hold, the baseband combiner  $\hat{\mathbf{W}}_{\text{BB}}^*$  and precoder  $\hat{\mathbf{F}}_{\text{BB}}^*$  that maximize the spectral efficiency in (6) for given  $\mathbf{H}_{\text{eff}}^* = \mathbf{H}_{\text{eff}}^*$  are

$$\hat{\mathbf{W}}_{\text{BB}}^* = [\mathbf{U}_{\text{eff}}^*]_{:,1:N_s}, \quad \hat{\mathbf{F}}_{\text{BB}}^* = [\mathbf{V}_{\text{eff}}^*]_{:,1:N_s} (\mathbf{P}_{\text{eff}}^*)^{1/2}, \quad (50)$$

where the SVD of  $\mathbf{H}_{\text{eff}}^*$  is expressed as  $\mathbf{H}_{\text{eff}}^* = \mathbf{U}_{\text{eff}}^* \boldsymbol{\Sigma}_{\text{eff}}^* (\mathbf{V}_{\text{eff}}^*)^{\text{H}}$ . The power allocation matrix  $(\mathbf{P}_{\text{eff}}^*)^{1/2}$  is given by  $(\mathbf{P}_{\text{eff}}^*)^{1/2} = \text{diag}([\sqrt{P_1^*}, \dots, \sqrt{P_{N_s}^*}])$ , where  $P_l^* = \left(\frac{1}{\eta^*} - \frac{\sigma_n^2}{\|\boldsymbol{\Sigma}_{\text{eff}}^*\|_{l,l}}\right)^+$ ,  $\forall l \in \{1, \dots, N_s\}$ , and  $\eta^*$  is chosen such that  $\sum_{l=1}^{N_s} P_l^* = P_{\text{TX}}$ . As both  $\mathbf{W}_{\text{RF}}^*$  and  $\mathbf{F}_{\text{RF}}^*$  have UPA array response vectors in their respective columns,  $(\mathbf{W}_{\text{RF}}^*)^{\text{H}} \mathbf{W}_{\text{RF}}^*$  and  $(\mathbf{F}_{\text{RF}}^*)^{\text{H}} \mathbf{F}_{\text{RF}}^*$  each approach  $\mathbf{I}_{N_r^{\text{RF}}}$  and  $\mathbf{I}_{N_t^{\text{RF}}}$  as  $N_t, N_r \rightarrow \infty$ . Therefore, using  $\hat{\mathbf{W}}_{\text{BB}}^*$  and  $\hat{\mathbf{F}}_{\text{BB}}^*$  as the baseband combiner and precoder is nearly optimal in mmWave systems, where large antenna arrays are employed at the TX and RX. Note that, while  $\mathbf{W}_{\text{RF}}^* \mathbf{W}_{\text{BB}}^*$  can be directly used as the hybrid combiner, there is no guarantee that the hybrid precoder  $\mathbf{F}_{\text{RF}}^* \hat{\mathbf{F}}_{\text{BB}}^*$  satisfies the transmit power constraint (5c) of the problem (P1), i.e.,

$\|\mathbf{F}_{\text{RF}}^* \hat{\mathbf{F}}_{\text{BB}}^*\|_{\text{F}}^2$  might be greater than  $P_{\text{TX}}$ . With this difference in mind, we adopt  $\mathbf{W}_{\text{BB}}^* = \hat{\mathbf{W}}_{\text{BB}}^*$  and  $\mathbf{F}_{\text{BB}}^* = \gamma^* \hat{\mathbf{F}}_{\text{BB}}^*$  as the baseband combiner and precoder, where

$$\gamma^* = \frac{\sqrt{P_{\text{TX}}}}{\|\mathbf{F}_{\text{RF}}^* \hat{\mathbf{F}}_{\text{BB}}^*\|_{\text{F}}} \quad (51)$$

is the normalization factor that ensures the transmit power constraint is met with equality, i.e.,  $\|\mathbf{F}_{\text{RF}}^* \mathbf{F}_{\text{BB}}^*\|_{\text{F}}^2 = P_{\text{TX}}$ . Since the asymptotic orthogonality of UPA array response vectors guarantees that  $\mathbf{F}_{\text{BB}}^*$  converges to  $\hat{\mathbf{F}}_{\text{BB}}^*$  as  $N_{\text{t}} \rightarrow \infty$ , we can conclude from (49) that the proposed hybrid precoder  $\mathbf{F}_{\text{RF}}^* \mathbf{F}_{\text{BB}}^*$  and combiner  $\mathbf{W}_{\text{RF}}^* \mathbf{W}_{\text{BB}}^*$  achieve spectral efficiency that asymptotically approaches  $R_{\text{max}}(\mathbf{H}_{\text{eff}}^*)$ , or equivalently  $R_{\text{max}}(\mathbf{H}_{\text{tot}}^*)$ , as  $N_{\text{t}}, N_{\text{r}}, M \rightarrow \infty$ . Therefore, in typical IRS-aided mmWave MIMO systems with a large number of antennas and IRS elements, the proposed hybrid beamformer design can perform close to the optimal fully-digital beamformer design, providing the systems with considerable benefits in terms of cost and energy efficiency.

#### IV. EXTENSION OF JOINT DESIGN TO MIMO-OFDM SYSTEMS

As one of the key features of mmWave communications is the usage of large bandwidth, it is important to investigate the design of IRS reflection matrix and hybrid beamformer for frequency-selective mmWave channels. In this section, we extend the proposed joint design of IRS reflection pattern and hybrid beamformer in Section III to broadband MIMO-OFDM systems.

##### A. System Model and Problem Formulation

Consider an IRS-aided MIMO-OFDM system where the TX performs digital precoding to the symbol vector  $\mathbf{s}[k] \in \mathbb{C}^{N_{\text{s}} \times 1}$  in the frequency domain by using the baseband precoder  $\mathbf{F}_{\text{BB}}[k] \in \mathbb{C}^{N_{\text{t}}^{\text{RF}} \times N_{\text{s}}}$  at each subcarrier  $k \in \{0, \dots, K-1\}$ . The precoded symbol vector is then transformed into the time domain through the  $K$ -point inverse fast Fourier transform (FFT) followed by cyclic prefix (CP) addition at each of the  $N_{\text{t}}^{\text{RF}}$  RF chains. Subsequently, the TX applies the analog precoder  $\mathbf{F}_{\text{RF}}$  to the transformed vector to produce the final transmitted signal. We assume that  $\mathbf{s}[k]$  satisfies  $\mathbb{E}[\mathbf{s}[k]\mathbf{s}[k]^{\text{H}}] = \mathbf{I}_{N_{\text{s}}}$ , and that the TX is subject to the per-subcarrier power constraint, i.e.,  $\|\mathbf{F}_{\text{RF}}\mathbf{F}_{\text{BB}}[k]\|_{\text{F}}^2 \leq P_{\text{TX}}[k]$ . The received signal at the subcarrier  $k$  can be expressed as

$$\begin{aligned} \mathbf{y}[k] &= (\mathbf{H}_{\text{TR}}[k] + \mathbf{H}_{\text{IR}}[k]\Phi\mathbf{H}_{\text{TI}}[k])\mathbf{F}_{\text{RF}}\mathbf{F}_{\text{BB}}[k]\mathbf{s}[k] + \mathbf{n}[k] \\ &= \mathbf{H}_{\text{tot}}[k]\mathbf{F}_{\text{RF}}\mathbf{F}_{\text{BB}}[k]\mathbf{s}[k] + \mathbf{n}[k] \end{aligned} \quad (52)$$

where  $\mathbf{H}_{\text{TR}}[k] \in \mathbb{C}^{N_{\text{r}} \times N_{\text{t}}}$ ,  $\mathbf{H}_{\text{TI}}[k] \in \mathbb{C}^{M \times N_{\text{t}}}$ , and  $\mathbf{H}_{\text{IR}}[k] \in \mathbb{C}^{N_{\text{r}} \times M}$  denote the frequency-domain channel matrices at the subcarrier  $k$  from the TX to RX, from the TX to IRS, and from the IRS to RX, respectively. The total combined channel matrix at the subcarrier  $k$  from the TX to RX is denoted by  $\mathbf{H}_{\text{tot}}[k] = \mathbf{H}_{\text{TR}}[k] + \mathbf{H}_{\text{IR}}[k]\Phi\mathbf{H}_{\text{TI}}[k]$ , and the AWGN vector  $\mathbf{n}[k]$  has entries that are i.i.d with  $\mathcal{CN}(0, \sigma_n^2)$ . The RX first applies the analog combiner  $\mathbf{W}_{\text{RF}}$  to the received signal in the time domain, and then transforms it into the frequency

domain by removing the CP and performing the  $K$ -point FFT at each of its  $N_{\text{r}}^{\text{RF}}$  RF chains. Finally, the RX uses the baseband combiner  $\mathbf{W}_{\text{BB}}[k] \in \mathbb{C}^{N_{\text{r}}^{\text{RF}} \times N_{\text{s}}}$  to obtain the processed received signal  $\tilde{\mathbf{y}}[k] = \mathbf{W}_{\text{BB}}[k]^{\text{H}}\mathbf{W}_{\text{RF}}^{\text{H}}\mathbf{y}[k]$  at each subcarrier  $k$ . For each  $i \in \{\text{TR}, \text{TI}, \text{IR}\}$ , the channel matrix  $\mathbf{H}_i[k]$  at the subcarrier  $k$  is expressed as [9], [31]

$$\mathbf{H}_i[k] = \sum_{q=0}^{N_{\text{path}}^i - 1} \alpha_{i,q} \mathbf{a}_{\text{r}}(\phi_{i,q}^{\text{r}}, \theta_{i,q}^{\text{r}}) \mathbf{a}_{\text{t}}(\phi_{i,q}^{\text{t}}, \theta_{i,q}^{\text{t}})^{\text{H}} e^{-j2\pi qk/K}. \quad (53)$$

The achievable spectral efficiency over the subcarrier  $k$  is given by

$$\begin{aligned} R[k] &= \log_2 \det(\mathbf{I}_{N_{\text{s}}} + \mathbf{R}_{\tilde{\mathbf{n}}[k]}^{-1} \mathbf{W}_{\text{BB}}[k]^{\text{H}} \mathbf{W}_{\text{RF}}^{\text{H}} \mathbf{H}_{\text{tot}}[k] \mathbf{F}_{\text{RF}} \mathbf{F}_{\text{BB}}[k] \\ &\quad \times \mathbf{F}_{\text{BB}}[k]^{\text{H}} \mathbf{F}_{\text{RF}}^{\text{H}} \mathbf{H}_{\text{tot}}[k]^{\text{H}} \mathbf{W}_{\text{RF}} \mathbf{W}_{\text{BB}}[k]), \end{aligned} \quad (54)$$

where  $\mathbf{R}_{\tilde{\mathbf{n}}[k]} = \sigma_n^2 \mathbf{W}_{\text{BB}}[k]^{\text{H}} \mathbf{W}_{\text{RF}}^{\text{H}} \mathbf{W}_{\text{RF}} \mathbf{W}_{\text{BB}}[k]$  is the covariance matrix of  $\tilde{\mathbf{n}}[k] = \mathbf{W}_{\text{BB}}[k]^{\text{H}} \mathbf{W}_{\text{RF}}^{\text{H}} \mathbf{n}[k]$ .

The problem of designing the IRS reflection pattern and hybrid beamformer that maximize the spectral efficiency of MIMO-OFDM systems can be formulated as

$$(P5) \quad \max_{\substack{\{\mathbf{W}_{\text{BB}}[k], \mathbf{F}_{\text{BB}}[k]\}_{k=0}^{K-1}, \\ \mathbf{W}_{\text{RF}}, \Phi, \mathbf{F}_{\text{RF}}}} \sum_{k=0}^{K-1} R[k] \quad (55a)$$

$$\text{subject to } \Phi = \text{diag}([e^{j\theta_1}, \dots, e^{j\theta_M}]), \quad (55b)$$

$$\|\mathbf{F}_{\text{RF}}\mathbf{F}_{\text{BB}}[k]\|_{\text{F}}^2 \leq P_{\text{TX}}[k], \quad (55c)$$

$$|[\mathbf{W}_{\text{RF}}]_{m,n}| = 1/\sqrt{N_{\text{r}}}, \forall m, n, \quad (55d)$$

$$|[\mathbf{F}_{\text{RF}}]_{m,n}| = 1/\sqrt{N_{\text{t}}}, \forall m, n. \quad (55e)$$

Following the similar steps used to derive the problem (P3) in Section III-A, we can formulate the effective channel design problem for MIMO-OFDM systems as

$$(P6) \quad \max_{\mathbf{W}_{\text{RF}}, \Phi, \mathbf{F}_{\text{RF}}} \sum_{k=0}^{K-1} R_{\text{max}}(\mathbf{H}_{\text{eff}}[k]) \quad (56a)$$

$$\text{subject to } \Phi = \text{diag}([e^{j\theta_1}, \dots, e^{j\theta_M}]), \quad (56b)$$

$$|[\mathbf{W}_{\text{RF}}]_{m,n}| = 1/\sqrt{N_{\text{r}}}, \forall m, n, \quad (56c)$$

$$|[\mathbf{F}_{\text{RF}}]_{m,n}| = 1/\sqrt{N_{\text{t}}}, \forall m, n, \quad (56d)$$

$$\mathbf{W}_{\text{RF}}^{\text{H}} \mathbf{W}_{\text{RF}} = \mathbf{I}_{N_{\text{r}}^{\text{RF}}}, \mathbf{F}_{\text{RF}}^{\text{H}} \mathbf{F}_{\text{RF}} = \mathbf{I}_{N_{\text{t}}^{\text{RF}}}, \quad (56e)$$

where  $R_{\text{max}}(\mathbf{H}_{\text{eff}}[k])$  denotes the maximum achievable spectral efficiency under the effective channel  $\mathbf{H}_{\text{eff}}[k] = \mathbf{W}_{\text{RF}}^{\text{H}} \mathbf{H}_{\text{tot}}[k] \mathbf{F}_{\text{RF}}$  at the subcarrier  $k$ . Note that, because both analog precoding and combining are performed after the inverse FFT operation,  $\mathbf{F}_{\text{RF}}$  and  $\mathbf{W}_{\text{RF}}$  are set to be identical for all the subcarriers. Similarly, the design of  $\Phi$  must take the channel matrices of all the subcarriers into account due to the lack of baseband processing capabilities at the IRS [20], [25]. These two characteristics of MIMO-OFDM systems make it impossible to directly apply the joint design proposed in Section III to frequency-selective mmWave channels.

##### B. IRS Reflection Pattern Design for MIMO-OFDM Systems

To tackle the effective channel design problem (P6) for MIMO-OFDM systems, we adopt the strategy similar to the



one described in Section III, where we first designed the IRS reflection matrix  $\Phi$ , and then constructed the analog precoder  $\mathbf{F}_{\text{RF}}$  and combiner  $\mathbf{W}_{\text{RF}}$  accordingly. We first define the complex gain matrix  $\mathbf{G}_i[k]$  for the mmWave channel  $\mathbf{H}_i[k]$  in (53) as

$$\mathbf{G}_i[k] = \text{diag} \left( [\alpha_{i,0}, \dots, \alpha_{i,N_{\text{path}}^i-1} \cdot e^{-j2\pi(N_{\text{path}}^i-1)k/K}] \right), \quad (57)$$

where, without loss of generality, we assume that  $|\mathbf{G}_i[k]_{m,m}| \geq |\mathbf{G}_i[k]_{n,n}|, \forall m, n \in \{1, \dots, N_{\text{path}}^i\}$  such that  $m < n$ . We can then express the decomposition of  $\mathbf{H}_i[k]$  as  $\mathbf{H}_i[k] = \mathbf{A}_i^i \mathbf{G}_i[k] (\mathbf{A}_i^i)^H$ , which has the identical structure as that of  $\mathbf{H}_i$  in (12). Therefore, by following the similar steps used to derive (32), we can show that  $\mathbf{H}_{\text{tot}}^*[k] = \mathbf{H}_{\text{TR}}[k] + \mathbf{H}_{\text{IR}}[k] \Phi^* \mathbf{H}_{\text{TI}}[k]$  satisfies

$$\begin{aligned} & \mathbf{H}_{\text{tot}}^*[k] (\mathbf{H}_{\text{tot}}^*[k])^H \\ & \rightarrow \sum_{s=0}^{N_{\text{path}}^{\text{TR}}-1} |\alpha_{\text{TR},s}|^2 \mathbf{a}_r(\phi_{\text{TR},s}^r, \theta_{\text{TR},s}^r) \mathbf{a}_r(\phi_{\text{TR},s}^r, \theta_{\text{TR},s}^r)^H \\ & \quad + |\alpha_{\text{TI},0}|^2 |\alpha_{\text{IR},0}|^2 \mathbf{a}_r(\phi_{\text{IR},0}^r, \theta_{\text{IR},0}^r) \mathbf{a}_r(\phi_{\text{IR},0}^r, \theta_{\text{IR},0}^r)^H, \quad (58) \end{aligned}$$

as  $N_t, M \rightarrow \infty$ , where  $\Phi^* = \text{diag}(\mathbf{v}^*)$  is the IRS reflection matrix proposed in Section III-B, and  $\mathbf{v}^*$  is given in (37). Since (32) and (58) indicate that  $\mathbf{H}_{\text{tot}}^*[k] (\mathbf{H}_{\text{tot}}^*[k])^H$  and  $\mathbf{H}_{\text{tot}}^* (\mathbf{H}_{\text{tot}}^*)^H$  converge to the same matrix for each  $k \in \{0, \dots, K-1\}$ , the IRS reflection matrix  $\Phi^*$  has the same asymptotic effect on the eigenvalues of  $\mathbf{H}_{\text{tot}}^*[k] (\mathbf{H}_{\text{tot}}^*[k])^H$  as it does on those of  $\mathbf{H}_{\text{tot}}^* (\mathbf{H}_{\text{tot}}^*)^H$ . As the inequality in (42) guarantees that the asymptotic eigenvalue  $|\alpha_{\text{TI},0}|^2 |\alpha_{\text{IR},0}|^2$  of  $\mathbf{H}_{\text{tot}}^* (\mathbf{H}_{\text{tot}}^*)^H$  and  $\mathbf{H}_{\text{tot}}^*[k] (\mathbf{H}_{\text{tot}}^*[k])^H$  increases at least quadratically with the number of IRS elements  $M$ , it can be concluded that the proposed IRS reflection pattern design in Section III-B will provide both narrowband and broadband MIMO systems with considerable gains in spectral efficiency.

### C. Analog Beamformer Design for MIMO-OFDM Systems

In the previous subsection, we showed that every frequency-domain channel matrix  $\mathbf{H}_i[k]$  at the subcarrier  $k$  shares the same receive array response matrix  $\mathbf{A}_i^i$  and transmit array response matrix  $\mathbf{A}_i^t$ . In this subsection, we exploit this particular property of frequency-selective mmWave channels to extend the proposed analog beamformer design in Section III-C to MIMO-OFDM systems. With  $\Phi = \Phi^*$ , the effective channel design problem (P6) is simplified as

$$(P7) \quad \max_{\mathbf{W}_{\text{RF}}, \mathbf{F}_{\text{RF}}} \sum_{k=0}^{K-1} R_{\max}(\mathbf{W}_{\text{RF}}^H \mathbf{H}_{\text{tot}}^*[k] \mathbf{F}_{\text{RF}}) \quad (59a)$$

$$\text{subject to} \quad \|\mathbf{W}_{\text{RF}}\|_{m,n} = 1/\sqrt{N_r}, \quad \forall m, n, \quad (59b)$$

$$\|\mathbf{F}_{\text{RF}}\|_{m,n} = 1/\sqrt{N_t}, \quad \forall m, n, \quad (59c)$$

$$\mathbf{W}_{\text{RF}}^H \mathbf{W}_{\text{RF}} = \mathbf{I}_{N_r^{\text{RF}}}, \quad \mathbf{F}_{\text{RF}}^H \mathbf{F}_{\text{RF}} = \mathbf{I}_{N_t^{\text{RF}}}. \quad (59d)$$

Let  $\mathbf{F}_{\text{RF},k^*}^* \in \mathbb{C}^{N_t \times N_t^{\text{RF}}}$  and  $\mathbf{W}_{\text{RF},k^*}^* \in \mathbb{C}^{N_r \times N_r^{\text{RF}}}$  denote the analog precoder and combiner obtained by applying the proposed analog beamformer design in Section III-C to  $\mathbf{H}_{\text{tot}}^*[k^*]$  for some  $k^* \in \{0, \dots, K-1\}$ , i.e., the columns of  $\mathbf{F}_{\text{RF},k^*}^*$  and  $\mathbf{W}_{\text{RF},k^*}^*$  are each set as the column vectors of  $\mathbf{A}_t$  with the

$N_t^{\text{RF}}$  largest quadratic norm  $\|\cdot\|_{(\mathbf{H}_{\text{tot}}^*[k^*])^H \mathbf{H}_{\text{tot}}^*[k^*]}$  and those of  $\mathbf{A}_r$  with the  $N_r^{\text{RF}}$  largest quadratic norm  $\|\cdot\|_{\mathbf{H}_{\text{tot}}^*[k^*] (\mathbf{H}_{\text{tot}}^*[k^*])^H}$ . Note that, for any  $k \in \{0, \dots, K-1\}$ , the problems (P4) and (P7) have exactly the same structure if the objective function of (P7) is replaced by  $R_{\max}(\mathbf{W}_{\text{RF}}^H \mathbf{H}_{\text{tot}}^*[k] \mathbf{F}_{\text{RF}})$ . Furthermore, as discussed in Section IV-B,  $\mathbf{H}_{\text{tot}}^*[k] (\mathbf{H}_{\text{tot}}^*[k])^H$  and  $\mathbf{H}_{\text{tot}}^* (\mathbf{H}_{\text{tot}}^*)^H$  converge to the same matrix as  $N_t, M \rightarrow \infty$ . Likewise, it can be shown that  $(\mathbf{H}_{\text{tot}}^*[k])^H \mathbf{H}_{\text{tot}}^*[k]$  and  $(\mathbf{H}_{\text{tot}}^*)^H \mathbf{H}_{\text{tot}}^*$  converge to the same  $N_t \times N_t$  matrix as  $N_r, M \rightarrow \infty$ . Therefore, it follows from (49) that, for each  $k \in \{0, \dots, K-1\}$ ,  $R_{\max}((\mathbf{W}_{\text{RF},k^*}^*)^H \mathbf{H}_{\text{tot}}^*[k] \mathbf{F}_{\text{RF},k^*}^*)$  asymptotically approaches the maximum achievable spectral efficiency  $R_{\max}(\mathbf{H}_{\text{tot}}^*[k])$  under  $\mathbf{H}_{\text{tot}}^*[k]$ . Since Proposition 3 implies that  $R_{\max}(\mathbf{W}_{\text{RF}}^H \mathbf{H}_{\text{tot}}^*[k] \mathbf{F}_{\text{RF}}) \leq R_{\max}(\mathbf{H}_{\text{tot}}^*[k])$  for each feasible solution  $\{\mathbf{W}_{\text{RF}}, \mathbf{F}_{\text{RF}}\}$  of the problem (P7), we have that  $\{\mathbf{W}_{\text{RF}} = \mathbf{W}_{\text{RF},k^*}^*, \mathbf{F}_{\text{RF}} = \mathbf{F}_{\text{RF},k^*}^*\}$  approaches the optimal solution of (P7) as  $N_t, N_r, M \rightarrow \infty$ .

With these formulations in mind, we now explain the analog beamformer design for frequency-selective mmWave channels. First, we use the analog beamformer design proposed in Section III-C to create the block matrices  $\mathbf{F}_{\text{RF}}^{\text{block}} \in \mathbb{C}^{N_t \times K N_t^{\text{RF}}}$  and  $\mathbf{W}_{\text{RF}}^{\text{block}} \in \mathbb{C}^{N_r \times K N_r^{\text{RF}}}$ , where

$$\begin{aligned} \mathbf{F}_{\text{RF}}^{\text{block}} &= [\mathbf{F}_{\text{RF},0}^* \quad \mathbf{F}_{\text{RF},1}^* \quad \dots \quad \mathbf{F}_{\text{RF},K-1}^*], \\ \mathbf{W}_{\text{RF}}^{\text{block}} &= [\mathbf{W}_{\text{RF},0}^* \quad \mathbf{W}_{\text{RF},1}^* \quad \dots \quad \mathbf{W}_{\text{RF},K-1}^*]. \quad (60) \end{aligned}$$

Then, among the column vectors of  $\mathbf{A}_t$ , we select the  $N_t^{\text{RF}}$  vectors that appear most frequently in the columns of  $\mathbf{F}_{\text{RF}}^{\text{block}}$  and place them in the columns of  $\mathbf{F}_{\text{RF}}^*$ . Similarly, among the column vectors of  $\mathbf{A}_r$ , we choose the  $N_r^{\text{RF}}$  vectors that appear most frequently in the columns of  $\mathbf{W}_{\text{RF}}^{\text{block}}$  to construct  $\mathbf{W}_{\text{RF}}^*$ . Analogous to (49), we have

$$\sum_{k=0}^{K-1} R_{\max}(\mathbf{H}_{\text{eff}}^*[k]) \rightarrow \sum_{k=0}^{K-1} R_{\max}(\mathbf{H}_{\text{tot}}^*[k]), \quad (61)$$

as  $N_t, N_r, M \rightarrow \infty$ , where  $\mathbf{H}_{\text{eff}}^*[k] = (\mathbf{W}_{\text{RF}}^*)^H \mathbf{H}_{\text{tot}}^*[k] \mathbf{F}_{\text{RF}}^*$ . The result in (61) demonstrates that the proposed analog precoder  $\mathbf{F}_{\text{RF}}^*$  and combiner  $\mathbf{W}_{\text{RF}}^*$  are asymptotically optimal for the problem (P7), and thus are highly effective in practical mmWave MIMO-OFDM systems.

### D. Baseband Beamformer Design for MIMO-OFDM Systems

In contrast to the IRS reflection matrix and analog precoder/combiner, the baseband precoder and combiner can be designed differently for each subcarrier. This flexibility greatly simplifies the generalization of the proposed baseband beamformer design from narrowband to broadband MIMO systems. That is, at each subcarrier  $k \in \{0, \dots, K-1\}$ , we can directly utilize the baseband beamformer design in Section III-D to construct the baseband precoder  $\mathbf{F}_{\text{BB}}^*[k] \in \mathbb{C}^{N_t^{\text{RF}} \times N_s}$  and combiner  $\mathbf{W}_{\text{BB}}^*[k] \in \mathbb{C}^{N_r^{\text{RF}} \times N_s}$  that asymptotically attain the maximum achievable spectral efficiency  $R_{\max}(\mathbf{H}_{\text{eff}}^*[k])$  under  $\mathbf{H}_{\text{eff}}^*[k] = (\mathbf{W}_{\text{RF}}^*)^H \mathbf{H}_{\text{tot}}^*[k] \mathbf{F}_{\text{RF}}^*$ . Denoting the SVD of  $\mathbf{H}_{\text{eff}}^*[k]$  as  $\mathbf{H}_{\text{eff}}^*[k] = \mathbf{U}_{\text{eff}}^*[k] \Sigma_{\text{eff}}^*[k] (\mathbf{V}_{\text{eff}}^*[k])^H$ , we can express  $\mathbf{F}_{\text{BB}}^*[k]$  and  $\mathbf{W}_{\text{BB}}^*[k]$  as

$$\begin{aligned} \mathbf{F}_{\text{BB}}^*[k] &= \gamma^*[k] [\mathbf{V}_{\text{eff}}^*[k]]_{:,1:N_s} (\mathbf{P}_{\text{eff}}^*[k])^{1/2}, \\ \mathbf{W}_{\text{BB}}^* &= [\mathbf{U}_{\text{eff}}^*[k]]_{:,1:N_s}, \quad (62) \end{aligned}$$

where  $(\mathbf{P}_{\text{eff}}^*[k])^{1/2} = \text{diag}\left(\left[\sqrt{P_1^*[k]}, \dots, \sqrt{P_{N_s}^*[k]}\right]\right)$ ,  $P_l^*[k] = \left(\frac{1}{\eta^*[k]} - \frac{\sigma_n^2}{|\mathbf{\Sigma}_{\text{eff}}^*[k]_{l,l}|^2}\right)^+$ ,  $\forall l \in \{1, \dots, N_s\}$ , and  $\eta^*[k]$  is chosen such that  $\sum_{l=1}^{N_s} P_l^*[k] = P_{\text{TX}}[k]$ . Similar to  $\gamma^*$  in (51), the normalization factor  $\gamma^*[k]$  is defined as

$$\gamma^*[k] = \frac{\sqrt{P_{\text{TX}}[k]}}{\|\mathbf{F}_{\text{RF}}^*[\mathbf{V}_{\text{eff}}^*[k]]_{:,1:N_s}(\mathbf{P}_{\text{eff}}^*[k])^{1/2}\|_{\text{F}}}, \quad (63)$$

so that the transmit power constraint is met with equality at each subcarrier, i.e.,  $\|\mathbf{F}_{\text{RF}}^* \mathbf{F}_{\text{BB}}^*[k]\|_{\text{F}}^2 = P_{\text{TX}}[k]$ ,  $\forall k \in \{0, \dots, K-1\}$ . Since  $(\mathbf{F}_{\text{RF}}^*)^H \mathbf{F}_{\text{RF}}^* \rightarrow \mathbf{I}_{N_t^{\text{RF}}}$  and  $(\mathbf{W}_{\text{RF}}^*)^H \mathbf{W}_{\text{RF}}^* \rightarrow \mathbf{I}_{N_r^{\text{RF}}}$  as  $N_t, N_r \rightarrow \infty$ , it follows directly from the discussions in Section III-D and (61) that the proposed hybrid beamformer  $\{\mathbf{W}_{\text{RF}}^* \mathbf{W}_{\text{BB}}^*[k], \mathbf{F}_{\text{RF}}^* \mathbf{F}_{\text{BB}}^*[k]\}_{k=0}^{K-1}$  achieves spectral efficiency that approaches arbitrarily close to  $\sum_{k=0}^{K-1} R_{\text{max}}(\mathbf{H}_{\text{tot}}^*[k])$  as  $N_t, N_r, M \rightarrow \infty$ . Given that IRS-aided mmWave MIMO-OFDM systems typically employ a large number of antennas and IRS elements, it can be concluded that, even with a significantly reduced number of RF chains, the proposed hybrid beamformer can attain performance close to that of fully-digital beamformer, as will be demonstrated in Section VI.

## V. COMPLEXITY ANALYSIS OF PROPOSED JOINT DESIGNS

In this section, we analyze the computational complexities of the proposed joint designs of IRS reflection pattern and hybrid beamformer for narrowband and broadband mmWave MIMO systems. Since the systems of interest typically employ a large number of antennas and IRS elements, we assume throughout the analysis that  $N_t, N_r$ , and  $M$  are much greater than  $N_t^{\text{RF}}, N_r^{\text{RF}}$  and  $N_{\text{path}}^i, i \in \{\text{TR}, \text{TI}, \text{IR}\}$ . Under this assumption, the complexities of the proposed IRS design and hybrid beamformer design for narrowband MIMO systems are given by  $\mathcal{O}(N_t N_r M)$  and  $\mathcal{O}(N_t N_r + N_t^{\text{RF}} N_r^{\text{RF}} N_{\text{min}}^{\text{RF}})$ , respectively. Therefore, the proposed joint design for narrowband systems has the complexity of  $\mathcal{O}(N_t N_r M)$ . Similarly, the complexity of the proposed joint design for MIMO-OFDM systems is calculated to be  $\mathcal{O}(K N_t N_r M)$ .

Table I shows the comparison of the computational complexities of the proposed joint designs, MO-based design [26], and geometric mean decomposition (GMD)-based design [27]. Note that the table does not include the complexity of MO-based design in MIMO-OFDM systems as the design cannot be applied to frequency-selective channels. By smartly leveraging the structures of frequency-flat and frequency-selective mmWave channels, the proposed designs achieve the lowest complexity for both narrowband and broadband MIMO systems.

## VI. SIMULATION RESULTS

In this section, we present simulation results to demonstrate the effectiveness of the proposed joint designs of IRS reflection pattern and hybrid beamformer for narrowband and broadband MIMO systems. We assume that the TX equipped with a UPA of  $N_t = 8 \times 8 = 64$  antennas communicates  $N_s = 4$  data streams to the RX with a UPA of  $N_r = 4 \times 4 = 16$  antennas. The number of RF chains at the TX and RX are set to be

TABLE I  
COMPUTATIONAL COMPLEXITIES OF DIFFERENT DESIGNS

Systems	Design	Computational Complexity
Narrowband MIMO	Proposed	$\mathcal{O}(N_t N_r M)$
	MO-based [26]	$\mathcal{O}(N_t N_r M + N_t N_r \min(N_t, N_r))$
	GMD-based [27]	$\mathcal{O}(N_t N_r M + N_t N_r \min(N_t, N_r))$
MIMO-OFDM	Proposed	$\mathcal{O}(K N_t N_r M)$
	GMD-based [27]	$\mathcal{O}(K N_t N_r M + K N_t N_r \min(N_t, N_r))$

$N_t^{\text{RF}} = N_r^{\text{RF}} = 4$ . Unless otherwise specified, we assume that the IRS is equipped with a UPA of  $M = 16 \times 16 = 256$  passive elements and that  $\mathbf{H}_i$  contains  $N_{\text{path}}^i = 8$  propagation paths,  $\forall i \in \{\text{TR}, \text{TI}, \text{IR}\}$ . The distance  $d_{\text{TR}} \in [d_{\text{TI}} + d_{\text{IR}} - 10 \text{ m}, d_{\text{TI}} + d_{\text{IR}} \text{ m}]$  between the TX and RX follows a uniform distribution over its range given  $d_{\text{TI}}$  and  $d_{\text{IR}}$ , each of which are uniformly distributed over [50 m, 60 m] and [10 m, 20 m]. The distance-dependent path loss  $PL(d_i)$  is modeled as

$$PL(d_i) [\text{dB}] = \alpha + 10\beta \log_{10}(d_i) + \xi, \quad (64)$$

where  $\xi \sim \mathcal{N}(0, \sigma^2)$ . According to the experimental data for 28 GHz channels in [28], the parameters in (64) are set to be  $\alpha = 61.4, \beta = 2, \sigma = 5.8 \text{ dB}$  for a line-of-sight (LOS) path of  $\mathbf{H}_i$ , and  $\alpha = 72.0, \beta = 2.92, \sigma = 8.7 \text{ dB}$  for its non-line-of-sight (NLOS) paths. To evaluate the effectiveness of different IRS reflection pattern designs more accurately, we assume that each path of  $\mathbf{H}_{\text{TR}}$  is a NLOS path that passes through tinted-glass walls to experience an additional penetration loss of 40.1dB [32]. The element spacing and noise power are each set to be  $d = \lambda/2$  and  $\sigma_n^2 = -91 \text{ dBm}$ . Lastly, all the simulation results are averaged over 10,000 channel realizations.

### A. Narrowband MIMO Systems

In this subsection, we evaluate the performance of the proposed joint design of IRS reflection pattern and hybrid beamformer for narrowband MIMO systems. Fig. 2 shows the spectral efficiency achieved by the proposed design as a function of the transmit power constraint  $P_{\text{TX}}$ . We also plotted in Fig. 2 the performances of when the phase shift of each IRS element is randomly selected from  $[0, 2\pi)$  and when there is no IRS, each of which are labeled as ‘‘Random IRS’’ and ‘‘No IRS’’. The results show that, with hybrid beamforming, the proposed design outperforms MO-based and GMD-based designs that require higher complexities. In addition, the spectral efficiency of the proposed design with hybrid beamforming is almost the same as that with fully-digital beamforming, demonstrating the effectiveness of the hybrid beamformer design presented in Section III. In contrast, there is a significant performance gap between GMD-based design with hybrid beamforming and that with fully-digital beamforming. This is primarily because the design aims to construct hybrid beamformers that achieve low BERs instead of high achievable rates. It can also be observed that there are negligible differences among the spectral efficiency achieved by MO-based design, Random IRS, and No IRS. This indicates that, in order to obtain performance gains from IRS, it is

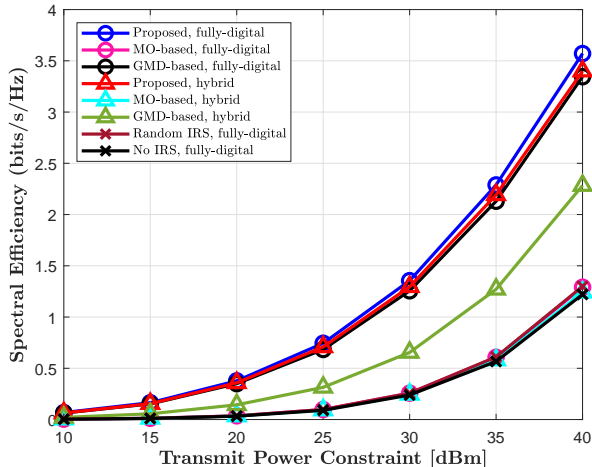


Fig. 2. Spectral efficiency achieved by different designs as a function of the transmit power constraint  $P_{TX}$ .

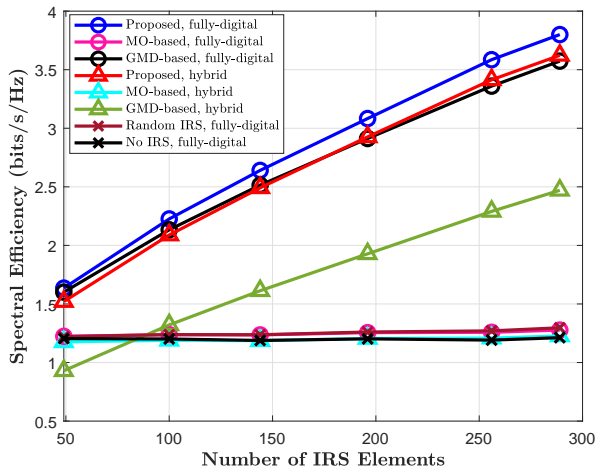


Fig. 3. Spectral efficiency achieved by different designs as a function of the number of IRS elements  $M$ .

important to take into account the presence of the direct channel and design the IRS reflection pattern carefully.

To investigate the impact that the number of IRS elements  $M$  has on the proposed design and other benchmarks, the spectral efficiency of different designs is plotted as a function of  $M$  in Fig. 3, where  $P_{TX} = 40$  dBm and  $M^h = M^v = \sqrt{M}$ . The figure shows that, as discussed in Section III-B, the spectral efficiency achieved by the proposed design significantly increases with  $M$ . In contrast, the performances of Random IRS and MO-based design do not improve monotonically with  $M$ . This indicates that, regardless of how many IRS elements are utilized, the judicious design of IRS reflection matrix is necessary to achieve spectral efficiency gains from IRS. Furthermore, the proposed design with hybrid beamforming performs just as well as that with fully-digital beamforming at all values of  $M$ , while GMD-based design requires fully-digital beamformers to perform comparably to the proposed design. This result demonstrates that the proposed joint design

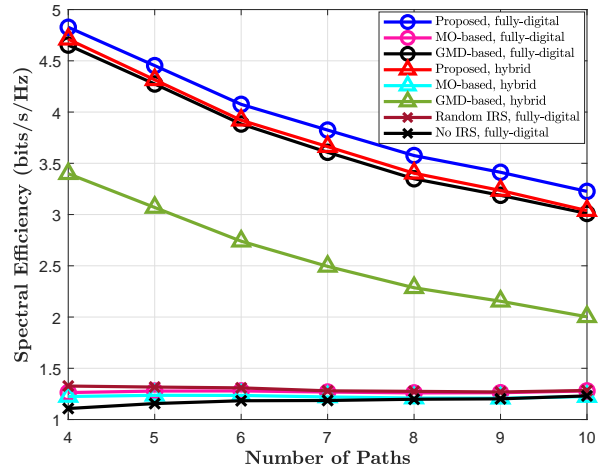


Fig. 4. Spectral efficiency achieved by different designs as a function of the number of paths  $N_{path}$ .

is highly suitable for mmWave MIMO systems, where fully-digital beamforming necessitates a large number of RF chains and thus is prohibitively expensive.

Fig. 4 plots the spectral efficiency of different designs against the number of paths  $N_{path} = N_{path}^i$ ,  $i \in \{TR, TI, IR\}$ , when  $P_{TX} = 40$  dBm. As shown in the figure, the spectral efficiency of the proposed design and GMD-based design increases as  $N_{path}$  decreases, while that of Random IRS and MO-based design does not change significantly according to  $N_{path}$ . This implies that the proposed design is well suited to mmWave systems in which communications are generally performed in environments with low scattering and small number of paths.

Since the phase shifters used to implement analog beamformers and IRS elements can only have finite resolution in practice [15], [33], we evaluate the performances of the proposed design and other benchmarks when each nonzero element of analog precoder/combiner and IRS reflection matrix is quantized with  $b$  bits according to the method described in [14]. Figs. 5 (a) and (b) each show the spectral efficiency of different designs versus  $P_{TX}$  when  $b = 1$  and  $b = 2$ . The results for higher values of  $b$  are omitted since the performance when  $b \geq 3$  has almost no difference from that when infinite-resolution phase shifters are assumed to be used [15]. As can be seen in Fig. 5 (a), the proposed design with  $b = 1$  outperforms MO-based design with infinite-resolution phase shifters, while GMD-based design with  $b = 1$  achieves lower spectral efficiency than MO-based design with  $b = 1$ . Also, as Fig. 5 (b) shows, the proposed design with  $b = 2$  achieves greater spectral efficiency than GMD-based design with infinite-resolution phase shifters at each value of  $P_{TX}$ . It can thus be concluded from the results in Fig. 5 that the proposed design can perform better than the other benchmarks in practical scenarios where finite-resolution phase shifters are employed for lower energy consumption and hardware complexity.

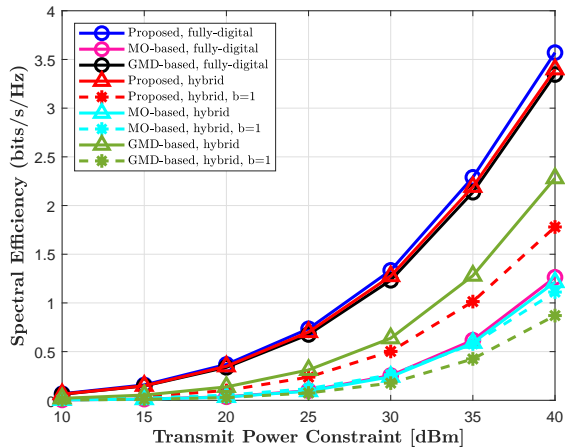
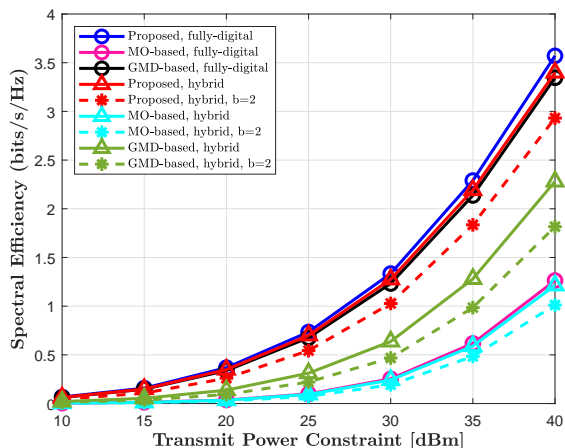
(a)  $b = 1$ (b)  $b = 2$ 

Fig. 5. Spectral efficiency achieved by different designs with finite-resolution phase shifters of quantization bits  $b$ .

### B. Broadband MIMO-OFDM Systems

In this subsection, we investigate the performance of the proposed joint design of IRS reflection pattern and hybrid beamformer for broadband MIMO-OFDM systems. We assume that equal power is allocated to each subcarrier, i.e.,  $P_{\text{TX}}[k] = P_{\text{TX}}/K, \forall k \in \{0, \dots, K-1\}$ . In Figs. 6 (a) and (b), the spectral efficiency that different designs achieve in MIMO-OFDM systems with  $K = 16$  and  $K = 64$  subcarriers is plotted as a function of  $P_{\text{TX}}$ . The figures show that the proposed design outperforms all the other benchmarks at both values of  $K$ , regardless of whether fully-digital or hybrid beamforming architectures are utilized. Also, the proposed design with hybrid beamforming achieves spectral efficiency very close to that of the design with fully-digital beamforming. In contrast, a significant performance gap exists between GMD-based design with fully-digital and hybrid beamforming, indicating that the proposed hybrid beamformer design is superior in terms of maximizing spectral efficiency. As demonstrated by the results in Fig. 6, the proposed joint design, which carefully exploits the angular sparsity of frequency-selective mmWave channels, is capable of providing substantial improvements in

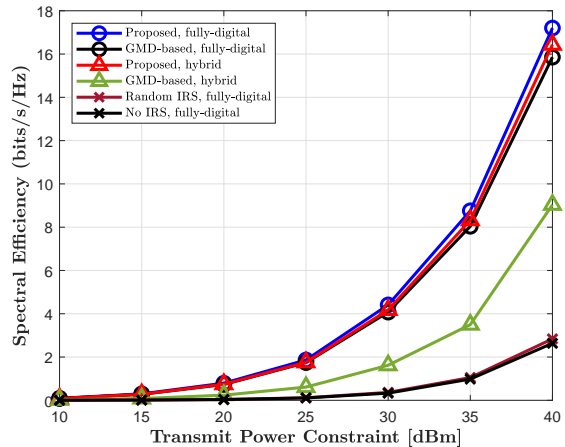
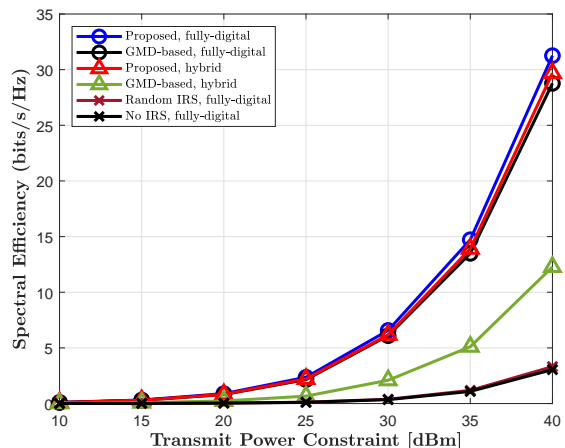
(a)  $K = 16$ (b)  $K = 64$ 

Fig. 6. Spectral efficiency of different designs in MIMO-OFDM systems with  $K$  subcarriers as a function of the transmit power constraint  $P_{\text{TX}}$ .

the spectral and energy efficiency of MIMO-OFDM systems.

## VII. CONCLUSIONS

In this paper, we studied narrowband and broadband IRS-aided mmWave MIMO systems with hybrid beamforming architectures. We first formulated the problem of designing the IRS reflection pattern and analog beamformer for narrowband MIMO systems into the effective channel design problem. By leveraging the sparse-scattering structure and large dimension of mmWave channels, we developed the joint design of IRS reflection pattern and hybrid beamformer for narrowband MIMO systems. We generalized the proposed joint design for narrowband MIMO systems to broadband MIMO-OFDM systems by carefully exploiting the sparsity of frequency-selective mmWave channels in the angular domain. Simulation results demonstrated that the proposed designs can provide the systems of interest with significant spectral efficiency gains and outperform the existing state-of-the-art designs while requiring lower computational complexity. Interesting future research directions include the investigation of the IRS reflection pattern and beamformer design that minimizes the

inter-user interference in IRS-aided multi-user systems with hybrid beamforming architectures.

#### APPENDIX A PROOF OF LEMMA 1

Let  $j \in \{0, \dots, N_{\text{path}}^{\text{TI}} - 1\}$ . Define a unitary matrix  $\mathbf{U}$  and a diagonal matrix  $\mathbf{\Lambda}$  such that  $\mathbf{H}_{\text{IR}}^{\text{H}} \mathbf{H}_{\text{IR}} = \mathbf{U} \mathbf{\Lambda} \mathbf{U}^{\text{H}}$ , where  $[\mathbf{\Lambda}]_{m,m}$  is necessarily an eigenvalue of  $\mathbf{H}_{\text{IR}}^{\text{H}} \mathbf{H}_{\text{IR}}$ ,  $\forall m \in \{1, \dots, M\}$ . Since it holds for each  $m$  that  $[\mathbf{\Lambda}]_{m,m} \leq \lambda_0(\mathbf{H}_{\text{IR}}^{\text{H}} \mathbf{H}_{\text{IR}})$ ,  $\|\mathbf{q}_j\|_2^2$  can be bounded as

$$\begin{aligned} \|\mathbf{q}_j\|_2^2 &= \mathbf{a}_r(\phi_{\text{TI},j}^r, \theta_{\text{TI},j}^r)^{\text{H}} \mathbf{\Phi}^{\text{H}} \mathbf{H}_{\text{IR}}^{\text{H}} \mathbf{H}_{\text{IR}} \mathbf{\Phi} \mathbf{a}_r(\phi_{\text{TI},j}^r, \theta_{\text{TI},j}^r) \\ &= \sum_{m=1}^M [\mathbf{\Lambda}]_{m,m} |[\mathbf{U}^{\text{H}} \mathbf{\Phi} \mathbf{a}_r(\phi_{\text{TI},j}^r, \theta_{\text{TI},j}^r)]_m|^2 \\ &\leq \lambda_0(\mathbf{H}_{\text{IR}}^{\text{H}} \mathbf{H}_{\text{IR}}) \|\mathbf{U}^{\text{H}} \mathbf{\Phi} \mathbf{a}_r(\phi_{\text{TI},j}^r, \theta_{\text{TI},j}^r)\|_2^2 = \lambda_0(\mathbf{H}_{\text{IR}}^{\text{H}} \mathbf{H}_{\text{IR}}), \end{aligned} \quad (65)$$

where the last equality follows from  $\|\mathbf{\Phi} \mathbf{a}_r(\phi_{\text{TI},j}^r, \theta_{\text{TI},j}^r)\|_2^2 = 1$ . We now prove the equality condition of the inequality (16) in Lemma 1. If  $\mathbf{H}_{\text{IR}}^{\text{H}} \mathbf{H}_{\text{IR}} \mathbf{\Phi} \mathbf{a}_r(\phi_{\text{TI},j}^r, \theta_{\text{TI},j}^r) = \lambda_0(\mathbf{H}_{\text{IR}}^{\text{H}} \mathbf{H}_{\text{IR}}) \mathbf{\Phi} \mathbf{a}_r(\phi_{\text{TI},j}^r, \theta_{\text{TI},j}^r)$ ,  $\|\mathbf{q}_j\|_2^2$  can be written as

$$\begin{aligned} \|\mathbf{q}_j\|_2^2 &= \lambda_0(\mathbf{H}_{\text{IR}}^{\text{H}} \mathbf{H}_{\text{IR}}) \|\mathbf{\Phi} \mathbf{a}_r(\phi_{\text{TI},j}^r, \theta_{\text{TI},j}^r)\|_2^2 \\ &= \lambda_0(\mathbf{H}_{\text{IR}}^{\text{H}} \mathbf{H}_{\text{IR}}). \end{aligned} \quad (66)$$

This completes the proof of Lemma 1.  $\square$

#### REFERENCES

- [1] Z. Pi and F. Khan, "An introduction to millimeter-wave mobile broadband systems," *IEEE Commun. Mag.*, vol. 49, no. 6, pp. 101–107, 2011.
- [2] Y. Niu *et al.*, "A survey of millimeter wave communications (mmWave) for 5G: opportunities and challenges," *Wireless Networks*, vol. 21, no. 6, pp. 2657–2676, 2015.
- [3] J. G. Andrews *et al.*, "What will 5G be?" *IEEE J. Sel. Areas Commun.*, vol. 32, no. 6, pp. 1065–1082, 2014.
- [4] A. L. Swindlehurst *et al.*, "Millimeter-wave massive MIMO: the next wireless revolution?" *IEEE Commun. Mag.*, vol. 52, no. 9, pp. 56–62, 2014.
- [5] E. G. Larsson *et al.*, "Massive MIMO for next generation wireless systems," *IEEE Commun. Mag.*, vol. 52, no. 2, pp. 186–195, 2014.
- [6] A. F. Molisch *et al.*, "Hybrid beamforming for massive MIMO: A survey," *IEEE Commun. Mag.*, vol. 55, no. 9, pp. 134–141, 2017.
- [7] I. Ahmed *et al.*, "A survey on hybrid beamforming techniques in 5G: Architecture and system model perspectives," *IEEE Commun. Surveys Tuts.*, vol. 20, no. 4, pp. 3060–3097, 2018.
- [8] O. E. Ayach *et al.*, "Spatially sparse precoding in millimeter wave MIMO systems," *IEEE Trans. Wireless Commun.*, vol. 13, no. 3, pp. 1499–1513, 2014.
- [9] X. Yu *et al.*, "Alternating minimization algorithms for hybrid precoding in millimeter wave MIMO systems," *IEEE J. Sel. Areas Commun.*, vol. 10, no. 3, pp. 485–500, 2016.
- [10] F. Sohrabi and W. Yu, "Hybrid analog and digital beamforming for mmWave OFDM large-scale antenna arrays," *IEEE J. Sel. Areas Commun.*, vol. 35, no. 7, pp. 1432–1443, 2017.
- [11] D. H. N. Nguyen *et al.*, "Hybrid MMSE precoding and combining designs for mmWave multiuser systems," *IEEE Access*, vol. 5, pp. 19 167–19 181, 2017.
- [12] J. Cong *et al.*, "Hybrid MMSE beamforming for multiuser millimeter-wave communication systems," *IEEE Commun. Lett.*, vol. 22, no. 11, pp. 2390–2393, 2018.
- [13] T. Lin *et al.*, "Hybrid beamforming for millimeter wave systems using the MMSE criterion," *IEEE Trans. Commun.*, vol. 67, no. 5, pp. 3693–3708, 2019.
- [14] J. Chen, "Hybrid beamforming with discrete phase shifters for millimeter-wave massive MIMO systems," *IEEE Trans. Veh. Technol.*, vol. 66, no. 8, pp. 7604–7608, 2017.
- [15] Z. Wang *et al.*, "Hybrid precoder and combiner design with low-resolution phase shifters in mmWave MIMO systems," *IEEE J. Sel. Topics Signal Process.*, vol. 12, no. 2, pp. 256–269, 2018.
- [16] J. Zhang *et al.*, "Prospective multiple antenna technologies for beyond 5G," *IEEE J. Sel. Areas Commun.*, vol. 38, no. 8, pp. 1637–1660, 2020.
- [17] Q. Wu and R. Zhang, "Intelligent reflecting surface enhanced wireless network via joint active and passive beamforming," *IEEE Trans. Wireless Commun.*, vol. 18, no. 11, pp. 5394–5409, 2019.
- [18] C. Huang *et al.*, "Holographic MIMO surfaces for 6G wireless networks: Opportunities, challenges, and trends," *IEEE Wireless Commun.*, vol. 27, no. 5, pp. 118–125, 2020.
- [19] Q. Wu and R. Zhang, "Towards smart and reconfigurable environment: Intelligent reflecting surface aided wireless network," *IEEE Commun. Mag.*, vol. 58, no. 1, pp. 106–112, 2020.
- [20] P. Yang *et al.*, "6G wireless communications: Vision and potential techniques," *IEEE Netw.*, vol. 33, no. 4, pp. 70–75, 2019.
- [21] W. Saad *et al.*, "A vision of 6G wireless systems: Applications, trends, technologies, and open research problems," *IEEE Netw.*, vol. 34, no. 3, pp. 134–142, 2020.
- [22] S. Kim *et al.*, "Practical channel estimation and phase shift design for intelligent reflecting surface empowered MIMO systems," 2021, *arXiv: 2104.14161*. [Online]. Available: <http://arxiv.org/abs/2104.14161>.
- [23] L. Dong and H. Wang, "Secure MIMO transmission via intelligent reflecting surface," *IEEE Wireless Commun. Lett.*, vol. 9, no. 6, pp. 787–790, 2020.
- [24] B. Ning *et al.*, "Beamforming optimization for intelligent reflecting surface assisted MIMO: A sum-path-gain maximization approach," *IEEE Wireless Commun. Lett.*, vol. 9, no. 7, pp. 1105–1109, 2020.
- [25] S. Zhang and R. Zhang, "Capacity characterization for intelligent reflecting surface aided MIMO communication," *IEEE J. Sel. Areas Commun.*, vol. 38, no. 8, pp. 1823–1838, 2020.
- [26] P. Wang *et al.*, "Joint transceiver and large intelligent surface design for massive MIMO mmWave systems," *IEEE Trans. Wireless Commun.*, vol. 20, no. 2, pp. 1052–1064, 2021.
- [27] K. Ying *et al.*, "GMD-based hybrid beamforming for large reconfigurable intelligent surface assisted millimeter-wave massive MIMO," *IEEE Access*, vol. 8, pp. 19 530–19 539, 2020.
- [28] M. R. Akdeniz *et al.*, "Millimeter wave channel modeling and cellular capacity evaluation," *IEEE J. Sel. Areas Commun.*, vol. 32, no. 6, pp. 1164–1179, 2014.
- [29] G. Casella and R. Berger, *Statistical Inference*. Cengage Learning, 2001.
- [30] Jinhui Chen, "When does asymptotic orthogonality exist for very large arrays?" in *Proc. IEEE Global Commun. Conf. Workshops (GLOBECOM)*, 2013, pp. 4146–4150.
- [31] J. Lee and Y. H. Lee, "AF relaying for millimeter wave communication systems with hybrid RF/baseband MIMO processing," in *Proc. IEEE Int. Conf. Commun. (ICC)*, 2014, pp. 5838–5842.
- [32] H. Zhao *et al.*, "28 GHz millimeter wave cellular communication measurements for reflection and penetration loss in and around buildings in New York city," in *Proc. IEEE Int. Conf. Commun. (ICC)*, 2013, pp. 5163–5167.
- [33] B. Di *et al.*, "Hybrid beamforming for reconfigurable intelligent surface based multi-user communications: Achievable rates with limited discrete phase shifts," *IEEE J. Sel. Areas Commun.*, vol. 38, no. 8, pp. 1809–1822, 2020.